

Oscillating-gradient spin-echo diffusion-weighted imaging (OGSE-DWI) with a limited number of oscillations: II. Asymptotics

Jeff Kershaw^{a,*} and Takayuki Obata^a

^a Applied MRI Research, National Institute of Radiological Sciences, QST, Chiba, Japan

*Corresponding author: len@qst.go.jp

Abstract

Oscillating-gradient spin-echo diffusion-weighted magnetic resonance imaging (OGSE-DWI) has been promoted as a promising technique for studying the microstructure of complex hydrated matter in the frequency domain. The target of the OGSE-DWI technique is the spectral density of molecular diffusion, $u_2(\omega)$, which is predicted to obey a set of asymptotic universality relations that are linked to the global organisation of the sample. So, in principle the complex microstructure of a medium can be classified by measuring the spectral density in its low- and high-frequency limits. However, due to practical limitations on the spectral resolution and range of the technique, it is not possible to directly sample the spectral density with OGSE-DWI. Rather, information about the spectral density can be obtained only indirectly through the quantities U_{kk} & U_{k0} , which are filtered representations of $u_2(\omega)$. The purpose of this study is to investigate how the universal behaviour of $u_2(\omega)$ emerges in the asymptotic behaviour of OGSE-DWI signal.

Keywords: oscillating gradient spin-echo, diffusion-weighted magnetic resonance imaging, finite motion-probing gradients, frequency domain, asymptotic expansion, structural universality, Mellin transform.

1. Introduction

Ever since it was first outlined by Stepisnik [1], oscillating-gradient spin-echo diffusion-weighted magnetic resonance imaging (OGSE-DWI) has been spoken of as a promising technique for studying the microstructure of complex hydrated matter. Although there are some variants (e.g. [2, 3, 4]), in its purest state the OGSE-DWI technique is distinguished by motion-probing gradients (MPGs) of the form

$$g(t) = G \cos(\omega_k t - \phi), \quad (1)$$

with amplitude G , frequency $\omega_k = 2\pi k/T$, arbitrary phase ϕ , duration T , time $0 \leq t \leq T$, and $k > 0$ an integer representing the number of oscillations. Under the assumption that k is very large, the conventional description for OGSE-DWI signal claimed that the spectral density of molecular diffusion, $u_2(\omega)$ (i.e. the Fourier transform of the velocity-autocorrelation function), can be directly measured at the selected frequency (e.g. [2, 4, 5, 6]). More recently, it has been pointed out that practical limitations on the duration and number of oscillations of a MPG restrict the spectral resolution and range of the technique [7]. Given that T and k must be finite, it was shown that the

signal equation for an oscillating single-harmonic MPG is

$$\ln s_k(T) = -\frac{\gamma^2 G^2 T}{4\omega_k^2} [U_{kk} + 2U_{k0} \sin^2 \phi], \quad (2)$$

where U_{kk} & U_{k0} are to be the measured quantities (note also that this equation is equivalent to Eq. (B5) in [11]). U_{kk} & U_{k0} are related to the spectral density via the relationship

$$U_{kl} = \int_0^\infty d\omega u_2(\omega) H_{kl}(\omega; T) \quad (3)$$

where

$$H_{kl}(\omega; T) = \frac{B_{kl} T (1 - \cos \omega T)}{[(\omega T)^2 - \varpi_k^2][(\omega T)^2 - \varpi_l^2]}, \quad (4)$$

$B_{kl} = 2(3\delta_{k,l} - 1)\varpi_k^2/\pi$, $\varpi_k = 2\pi k$, $\delta_{k,l}$ is the Kronecker delta, and l equals either 0 or k . In short, U_{kk} & U_{k0} are representations of $u_2(\omega)$ filtered by the functions $H_{kl}(\omega; T)$.

Rather than directly sampling the spectral density, Eqs. (2) & (3) imply that information about $u_2(\omega)$ can be obtained only indirectly through measurements of U_{kk} & U_{k0} . After applying Eq. (3) to three examples of $u_2(\omega)$ taken from the literature, it was suggested that U_{kk} provides a reasonable qualitative understanding of the spectral density for a particular system, while U_{k0} reflects the cumulative diffusion coefficient $D(T)$ of the system [7]. However, it remains to be demonstrated how such measurements can be used to quantify the microstructure of complex media. If $u_2(\omega)$ were a well-established function then the exact theoretical forms of U_{kk} & U_{k0} could be evaluated and fitted to the data to obtain estimates of the important parameters. Unfortunately, when making observations of real/natural systems it is unlikely that $u_2(\omega)$ will be known *a priori*. It is fortunate then that certain global features of a system might be quantified by observing the asymptotic behaviour of $u_2(\omega)$. In the low and high frequency limits it has been predicted that $u_2(\omega)$ behaves universally as [6, 8]¹

$$u_2(\omega) \sim \begin{cases} 2D_\infty + c_\infty \omega^\vartheta, & \omega \rightarrow 0 \\ 2D_0 - c_0 \omega^{-1/2}, & \omega \rightarrow \infty \end{cases} \quad (5)$$

where c_∞ is a constant that may depend on microscopic details of the system and $c_0 = \sqrt{2}(S/V) D_0^{3/2}/d$. For the low-frequency limit the global behaviour is captured in the dynamical exponent $\vartheta = (p + d)/2$, with p being a structural exponent characterising the global organisation of the microstructure in a d -dimensional medium. In the high-frequency limit, the inverse-square-root dependence on frequency is a feature that is universally true for complex media, which means that the surface-to-volume ratio, S/V , is a quantity that can be used to characterise the global properties of a medium. It is the purpose of this study to investigate how these global characteristics appear in the asymptotic behaviour of U_{k0} & U_{kk} .

The paper is organised so that the method used to derive asymptotic expansions for U_{k0} & U_{kk} is introduced first (Sec. 2), after which the method is demonstrated by applying it to several

¹It is common in the literature to associate the symbols D_∞ & D_0 with the low- & high-frequency limits, respectively, of a frequency-dependent diffusion metric. The notation originates from the association of the same symbols with the long- and short-time limits of various time-dependent diffusion metrics. For consistency, this work shall adopt the same convention of labeling coefficients involved in the low- & high-frequency limits with an index of ∞ & 0, respectively. The index will be a subscript if there are no other indices, otherwise the index will be a superscript.

examples (Sec. 3), before it is applied to achieve the intended goal (Sec. 4). Some discussion will then follow.

2. Asymptotics of U_{k0} & U_{kk}

2.1. Asymptotic variables

To obtain the asymptotic behaviour of $u_2(\omega)$ first recall that there is a time-scale characterising the response of every system. In fact, the response of a system may depend on several time scales, in which case the smallest and largest will determine the behaviour in the asymptotic limits. For simplicity, and without loss of generality, it shall be assumed here that the important time-scale in either limit is always represented by τ . The asymptotic behaviour of the system is obtained by expanding $u_2(\omega)$ in the limits $\omega\tau \rightarrow 0$ and $\omega\tau \rightarrow \infty$, corresponding to the low and high frequency regimes, respectively. Note that in this case ω is a continuous quantity that can be arbitrarily increased or decreased relative to τ to meet the requirement for each limit. For that reason the asymptotic tendency is often presented as $\omega \rightarrow 0$ or $\omega \rightarrow \infty$ when writing down the asymptotic behaviour of $u_2(\omega)$, leaving out the dependence of the asymptotic variable on τ .

The asymptotic behaviour of U_{k0} & U_{kk} can be similarly obtained by expanding with respect to $\omega_k\tau$. The observation frequency ω_k can be manipulated by varying either k or T . Unfortunately, it is not possible to unboundedly increase or decrease either of those parameters, which means that ω_k cannot be arbitrarily set to meet the requirement for observations in either of the asymptotic regimes. Therefore the value of τ relative to the accessible range of ω_k becomes important. As noted in [7], it is advantageous to choose T to be as long as possible in practice because it allows the widest range of accessible frequencies. Nevertheless, the range of k is limited, so it must actually be the value of T relative to τ that determines whether $\omega_k\tau$ matches the condition for either the low- or high-frequency regimes. With that understanding, from here on $\omega_k\tau$ and $\beta = T/\tau$ will be used interchangeably as the asymptotic variables of U_{k0} & U_{kk} , and it should also be understood that requiring the limits $\omega_k\tau \rightarrow 0$ and $\omega_k\tau \rightarrow \infty$ is equivalent to taking $\beta \rightarrow \infty$ and $\beta \rightarrow 0$, respectively.

2.2. The Mellin transform method

Returning to Eq. (3) now, to obtain the asymptotic behaviour of U_{kl} the obvious course of action is to evaluate the integral and then expand with respect to $\omega_k\tau$ (or β). However, it may be that the integral requires a lot of tedious work or is simply just too difficult to evaluate exactly. In that case a more direct alternative is to apply the Mellin transform method (MTM) for the asymptotic expansion of integrals [9]. Summarising its use for Eq. (3), after the variable change $v = \omega\tau$ the integral can be written in the dimensionless form

$$I_{kl}(\beta) = \frac{U_{kl}}{2D_0 B_{kl} \beta} = \int_0^\infty dv f(v) h_{kl}(\beta v) \quad (6)$$

where $f(v) = u_2(v/\tau)/2D_0$ and

$$h_{kl}(v) = \frac{1 - \cos v}{(v^2 - \varpi_k^2)(v^2 - \varpi_l^2)}.$$

For $s \in \mathbb{C}$ the Mellin transform of $h_{kl}(v)$, $M[h_{kl}; s]$, is well defined in the ordinary sense (Supporting Material, Sec. S-5). In contrast, other than the assumption that it is continuous, the

properties of $u_2(\omega)$ are usually unknown *a priori*, which means it is not generally true that the Mellin transform of $f(v)$, $M[f; s]$, exists in the ordinary sense. Choose instead an arbitrary real number $v_0 > 0$ so that $f(v) = f_1(v) + f_2(v)$ with

$$f_1(v) = \begin{cases} f(v), & 0 \leq v < v_0 \\ 0, & v_0 \leq v < \infty \end{cases} \quad (7)$$

and

$$f_2(v) = \begin{cases} 0, & 0 \leq v < v_0 \\ f(v), & v_0 \leq v < \infty. \end{cases} \quad (8)$$

Under these conditions the Mellin transforms of $f_1(v)$ & $f_2(v)$ do exist, and therefore the quantity $M[f_1; s] + M[f_2; s]$ is understood as the Mellin transform of $f(v)$ in the generalised sense. Now let $G_{lj}(s) = M[f_j; 1-s]M[h_{kl}; s]$ ($j = 1, 2$) where both $M[h_{kl}; s]$ and $M[f_j; 1-s]$ are analytic within the strip $a_{lj} < \text{Re } s < b_{lj}$ ($a_{lj}, b_{lj} \in \mathbb{R}$) of the complex plane. The poles s_n of $G_{lj}(s)$ lie outside of the analytic strip and may be organised into two sets, $\{s_n \leq a_{lj}\}$ and $\{s_n \geq b_{lj}\}$, according to whether $\text{Re } s_n$ lies to the left or right of the complex plane from the analytic strip. Then the series

$$I_{kl}^j(\beta) = \int_0^\infty dv f_j(v) h_{kl}(\beta v) \sim \begin{cases} \sum_{\{s_n \leq a_{lj}\}} \text{Res} \{ \beta^{-s} G_{lj}(s) \}, & \beta \rightarrow 0 \\ - \sum_{\{s_n \geq b_{lj}\}} \text{Res} \{ \beta^{-s} G_{lj}(s) \}, & \beta \rightarrow \infty \end{cases} \quad (9)$$

provide asymptotic expansions for $I_{kl}(\beta) = I_{kl}^1(\beta) + I_{kl}^2(\beta)$ as sums over the residues of $G_{lj}(s)$ at its poles. Terms in the series associated with poles having real parts closer to the analytic strip will in general dominate terms corresponding to poles sitting further away.

More detail on the Mellin transform and MTM has been included in the Supporting Material (Secs. S-1 & S-2).

2.3. The poles of $M[h_{kl}; s]$, $M[f_j; 1-s]$ and $G_{lj}(s)$

Evaluating the terms in the series of Eq. (9) is aided by the fact that the local behaviour of $M[h_{kl}; s]$ and $M[f_j; 1-s]$ near a pole is directly linked to the powers of v in expansions of $h_{kl}(v)$ and $f(v)$ about 0 and ∞ . For example, the function $h_{kl}(v)$ has the asymptotic expansions

$$h_{kl}(v) \sim \begin{cases} \sum_{n=0}^{\infty} h_{ln}^0 v^{2(n+\delta_{k,l})}, & v \rightarrow 0 \\ (1 - \cos v) \sum_{n=0}^{\infty} h_{ln}^\infty v^{-2(n+2)}, & v \rightarrow \infty \end{cases} \quad (10)$$

where

$$h_{ln}^0 = \frac{(-)^{n+1-\delta_{k,l}}}{\varpi_k^{2(1+\delta_{k,l})}} \sum_{m=0}^n \frac{(-)^m (1+m\delta_{k,l})}{\varpi_k^{2m} (2n-2m+2)!}$$

$$h_{ln}^\infty = (1+n\delta_{k,l}) \varpi_k^{2n}.$$

It follows from the properties of the Mellin transform that

$$M[h_{kl}; s] \sim \begin{cases} \frac{h_{ln}^0}{s + 2(n + \delta_{k,l})}, & s \rightarrow -2(n + \delta_{k,l}) \\ -\frac{h_{ln}^\infty}{s - 2(n + 2)}, & s \rightarrow 2(n + 2) \end{cases} \quad (11)$$

with $n = 0, 1, 2, \dots$. Notice that the poles of $M[h_{kl}; s]$ are all simple and equal to minus the powers of v in the asymptotic expansions.

For the case of $f(v)$, it is assumed that it may be expanded in power series about 0 and ∞ like so

$$f(v) \sim \begin{cases} \sum_{n=0}^{\infty} f_n^0 v^{\theta_{1n}}, & v \rightarrow 0 \\ \sum_{n=0}^{\infty} f_n^\infty v^{-\theta_{2n}}, & v \rightarrow \infty. \end{cases} \quad (12)$$

Here $\{\theta_{1n}\}$ and $\{\theta_{2n}\}$ are strictly monotonic increasing sequences of real numbers. In accordance with the definitions of $f_1(v)$ and $f_2(v)$ in Eqs. (7) & (8) above, it follows that

$$M[f_1; 1 - s] \sim -\frac{f_n^0}{s - \theta_{1n} - 1}, \quad s \rightarrow \theta_{1n} + 1 \quad (13)$$

$$M[f_2; 1 - s] \sim \frac{f_n^\infty}{s + \theta_{2n} - 1}, \quad s \rightarrow -\theta_{2n} + 1 \quad (14)$$

for $n = 0, 1, 2, \dots$. The poles of the $M[f_j; 1 - s]$ are also simple and, due to the shift in argument from s to $1 - s$, are equal to 1 plus the powers of v in the expansions of $f(v)$.

The pole sets of $G_{lj}(s)$ are composed from the poles of $M[f_j; 1 - s]$ and $M[h_{kl}; s]$. For $j = 1$, the analytic strips of $M[f_1; 1 - s]$ and $M[h_{kl}; s]$ intersect for $-2\delta_{k,l} < \text{Re } s < 1 + \theta_{10}$ so $a_{l1} = -2\delta_{k,l}$, $b_{l1} = 1 + \theta_{10}$ and the poles of $G_{l1}(s)$ are

$$\begin{aligned} \{s_n \leq a_{l1}\} &= \{-2(n + \delta_{k,l})\} \\ \{s_n \geq b_{l1}\} &= \{2(n + 2)\} \cup \{\theta_{1n} + 1\}. \end{aligned}$$

Likewise for $j = 2$, the analytic strips of $M[f_2; 1 - s]$ and $M[h_{kl}; s]$ intersect when $1 - \theta_{20} < \text{Re } s < 4$ so the poles of $G_{l2}(s)$ are

$$\begin{aligned} \{s_n \leq a_{l2}\} &= \{-2(n + \delta_{k,l})\} \cup \{-\theta_{2n} + 1\} \\ \{s_n \geq b_{l2}\} &= \{2(n + 2)\} \end{aligned}$$

with $a_{l2} = 1 - \theta_{20} = 1$ and $b_{l2} = 4$. Realising that there may be some overlap between the poles of the $M[f_j; 1 - s]$ and $M[h_{kl}; s]$, let Q_{l1} be a set containing all pairs of non-negative integers (p, r) such that $\theta_{1p} + 1 = 2(r + 2)$, and let P_{l1} & R_{l1} be sets containing all values of p & r , respectively, that are not included as part of one of the pairs in Q_{l1} . Similarly, let Q_{l2} contain non-negative integer pairs (p, r) such that $-\theta_{2p} + 1 = -2(r + \delta_{k,l})$, and let P_{l2} & R_{l2} be sets respectively consisting of the p & r that are not already elements of Q_{l2} . These definitions allow the poles in $\{s_n \geq b_{l1}\}$ and $\{s_n \leq a_{l2}\}$ to be organised into three disjoint sets. Moreover, as the poles of $M[h_{kl}; s]$ and the

$M[f_j; 1 - s]$ are all simple, it is easy to calculate the residues in Eq. (9) and use them to write $I_{kl}(\beta) = I_{kl}^P(\beta) + I_{kl}^Q(\beta) + I_{kl}^R(\beta)$ where

$$I_{kl}^P(\beta) \sim \begin{cases} \sum_{p \in P_{l2}} \beta^{\theta_{2p}-1} f_p^\infty M[h_{kl}; -\theta_{2p} + 1], & \beta \rightarrow 0 \\ \sum_{p \in P_{l1}} \beta^{-\theta_{1p}-1} f_p^0 M[h_{kl}; \theta_{1p} + 1], & \beta \rightarrow \infty \end{cases} \quad (15)$$

$$I_{kl}^R(\beta) \sim \begin{cases} \sum_{r \in R_{l2}} \beta^{2(r+\delta_{k,l})} h_{lr}^0 M[f; 2r + 2\delta_{k,l} + 1], & \beta \rightarrow 0 \\ \sum_{r \in R_{l1}} \beta^{-2(r+2)} h_{lr}^\infty M[f; -2r - 3], & \beta \rightarrow \infty \end{cases} \quad (16)$$

$$I_{kl}^Q(\beta) \sim \begin{cases} \sum_{(p,r) \in Q_{l2}} \beta^{\theta_{2p}-1} K_{lpr}^2 - \ln \beta \sum_{(p,r) \in Q_{l2}} \beta^{\theta_{2p}-1} h_{lr}^0 f_p^\infty, & \beta \rightarrow 0 \\ \sum_{(p,r) \in Q_{l1}} \beta^{-\theta_{1p}-1} K_{lpr}^1 + \ln \beta \sum_{(p,r) \in Q_{l1}} \beta^{-\theta_{1p}-1} h_{lr}^\infty f_p^0, & \beta \rightarrow \infty \end{cases} \quad (17)$$

$$K_{lpr}^1 = h_{lr}^\infty M[f_2; -\theta_{1p}] - \lim_{s \rightarrow \theta_{1p}+1} \frac{d}{ds} \{(s - \theta_{1p} - 1)^2 G_{l1}(s)\}$$

$$K_{lpr}^2 = h_{lr}^0 M[f_1; \theta_{2p}] + \lim_{s \rightarrow -\theta_{2p}+1} \frac{d}{ds} \{(s + \theta_{2p} - 1)^2 G_{l2}(s)\}$$

Note that the Mellin transform of $f(v)$ in $I_{kl}^R(\beta)$ is to be understood in the generalised sense.

The series in $I_{kl}^P(\beta)$ have terms proportional to $\beta^{\theta_{1p}-1}$ and $\beta^{-\theta_{2p}-1}$. Therefore, after multiplying by the factor of β from the central term in Eq. (6) and recalling that $\beta = \varpi_k/\omega_k\tau$, the effect of $I_{kl}^P(\beta)$ on the asymptotic behaviour of U_{kl} is to supply terms with the same powers of $\omega_k\tau$ that appear in an expansion of $u_2(\omega_k)$. In contrast, by the construction of R_{l1} and R_{l2} , $I_{kl}^R(\beta)$ provides terms to the asymptotic behaviour of U_{kl} that are qualitatively different to those in an expansion of $u_2(\omega_k)$. In some circumstances the qualitatively different behaviour of $I_{kl}^R(\beta)$ may dominate the qualitatively similar behaviour of $I_{kl}^P(\beta)$ so that the asymptotic response of the system is masked by the behaviour of the filters $H_{kl}(\omega; T)$.

Since the poles in Q_{l1} and Q_{l2} are second order, evaluation of the residues is a little more complicated, with the result that $I_{kl}^Q(\beta)$ can be organised into two separate sums (re Eq. (17)). The first of these has terms proportional to $\beta^{\theta_{1p}-1}$ and $\beta^{-\theta_{2p}-1}$ so its effect on the asymptotic behaviour of U_{kl} is similar to that of $I_{kl}^P(\beta)$. On the other hand, the terms in the second sum are multiplied by a factor of $\ln \beta$ so, like the case for $I_{kl}^R(\beta)$, the effect on the asymptotic behaviour of U_{kl} is qualitatively different to that of $u_2(\omega_k)$.

If the $M[f_j; 1 - s]$ have poles of 2nd or higher order, evaluation of the residues in $I_{kl}^P(\beta)$ and $I_{kl}^Q(\beta)$ will be more complicated and integer powers of $\ln \beta$ will appear. In contrast, evaluation of the terms in $I_{kl}^R(\beta)$ will not be altered because the elements of R_{l1} and R_{l2} will always be simple poles.

3. Application to three models

The method described in Sec. 2 is now applied to derive the asymptotic behaviour of U_{k0} & U_{kk} for three examples taken from the literature. A brief description for each model can be found in [7], as can the exact forms of U_{k0} & U_{kk} for the first two models. Details of the MTM applied to each model have been included in the Supporting Material (Secs. S-4 & S-5). The sets Q_{l1} & Q_{l2} are empty for all three models so only $I_{kl}^P(\beta)$ & $I_{kl}^R(\beta)$ contribute to the asymptotic behaviour. Each result contains the two most dominant terms from $I_{kl}^P(\beta)$ & $I_{kl}^R(\beta)$ together with the order of the next most significant term.

Model 1. Expanding $u_2(\omega)$ in the appropriate limits

$$\frac{u_2(\omega)}{2D_0} \sim \begin{cases} (1 - \eta) + \eta(\omega\tau)^2 + O(\omega\tau)^4, & \omega\tau \rightarrow 0 \\ 1 - \eta(\omega\tau)^{-2} + O(\omega\tau)^{-4}, & \omega\tau \rightarrow \infty. \end{cases} \quad (18)$$

The corresponding expansions for the measured quantities are

$$\frac{U_{k0}}{2D_0} \sim \begin{cases} (1 - \eta) + \frac{\eta}{\varpi_k}(\omega_k\tau)^3 + O(\omega_k\tau)^5, & \omega_k\tau \rightarrow 0 \\ 1 - \frac{\eta\varpi_k}{2}(\omega_k\tau)^{-1} + O(\omega_k\tau)^{-2}, & \omega_k\tau \rightarrow \infty \end{cases} \quad (19)$$

$$\frac{U_{kk}}{2D_0} \sim \begin{cases} (1 - \eta) + \eta(\omega_k\tau)^2 + O(\omega_k\tau)^3, & \omega_k\tau \rightarrow 0 \\ 1 - 3\eta(\omega_k\tau)^{-2} + O(\omega_k\tau)^{-3}, & \omega_k\tau \rightarrow \infty. \end{cases} \quad (20)$$

Model 2. Expansion of the spectral density for this model gives

$$\frac{u_2(\omega)}{2D_0} \sim \begin{cases} (1 - \zeta) + \frac{\zeta}{\sqrt{2}}(\omega\tau)^{1/2} + O(\omega\tau)^{3/2}, & \omega\tau \rightarrow 0 \\ 1 - \frac{\zeta}{\sqrt{2}}(\omega\tau)^{-1/2} + O(\omega\tau)^{-3/2}, & \omega\tau \rightarrow \infty. \end{cases} \quad (21)$$

Direct expansion of the exact results for U_{k0} & U_{kk} can be used to confirm that

$$\frac{U_{k0}}{2D_0} \sim \begin{cases} (1 - \zeta) + A_{01}^\infty \frac{\zeta}{\sqrt{2}}(\omega_k\tau)^{1/2} + O(\omega_k\tau)^{3/2}, & \omega_k\tau \rightarrow 0 \\ 1 - A_{01}^0 \frac{\zeta}{\sqrt{2}}(\omega_k\tau)^{-1/2} + O(\omega_k\tau)^{-1}, & \omega_k\tau \rightarrow \infty \end{cases} \quad (22)$$

$$A_{01}^\infty = \frac{2}{\pi k^{1/2}} - \frac{a_{ck}}{\varpi_k}, \quad A_{01}^0 = \frac{8k^{1/2}}{3} + \frac{a_{sk}}{\varpi_k}$$

$$\frac{U_{kk}}{2D_0} \sim \begin{cases} (1 - \zeta) + A_{k1}^\infty \frac{\zeta}{\sqrt{2}}(\omega_k\tau)^{1/2} + O(\omega_k\tau)^{3/2}, & \omega_k\tau \rightarrow 0 \\ 1 - A_{k1}^0 \frac{\zeta}{\sqrt{2}}(\omega_k\tau)^{-1/2} + O(\omega_k\tau)^{-3/2}, & \omega_k\tau \rightarrow \infty \end{cases} \quad (23)$$

$$A_{k1}^\infty = \frac{1}{\pi k^{1/2}} - \frac{a_{ck}}{2\varpi_k} + a_{sk}, \quad A_{k1}^0 = \frac{3a_{sk}}{2\varpi_k} + a_{ck}.$$

Here $a_{sk} = 2S(2k^{1/2})$ and $a_{ck} = 2C(2k^{1/2})$, where $S(z)$ and $C(z)$ are the Fresnel integrals.

Model 3. A description of how the following expansions of $u_2(\omega)$ were obtained for this model is contained in Sec. S-5 of the Supporting Material.

$$\frac{u_2(\omega)}{2D_0} \sim \begin{cases} \frac{1}{1+\zeta} + \frac{\sqrt{2}[\sqrt{1+\zeta}-1]}{(1+\zeta)^2}(\omega\tau)^{\frac{1}{2}} + O(\omega\tau)^{\frac{3}{2}}, & \omega\tau \rightarrow 0 \\ 1 - \frac{\zeta}{\sqrt{2}}(\omega\tau)^{-\frac{1}{2}} + O(\omega\tau)^{-\frac{3}{2}}, & \omega\tau \rightarrow \infty. \end{cases} \quad (24)$$

The leading terms in the final results are

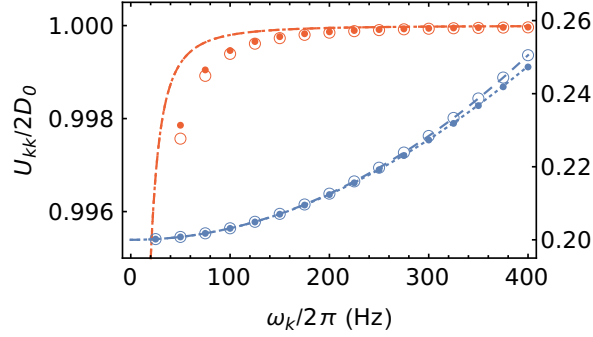
$$\frac{U_{k0}}{2D_0} \sim \begin{cases} \frac{1}{1+\zeta} + A_{01}^{\infty} \frac{\sqrt{2}[\sqrt{1+\zeta}-1]}{(1+\zeta)^2}(\omega_k\tau)^{\frac{1}{2}} + O(\omega_k\tau)^{\frac{3}{2}}, & \omega_k\tau \rightarrow 0 \\ 1 - A_{01}^0 \frac{\zeta}{\sqrt{2}}(\omega_k\tau)^{-\frac{1}{2}} + O(\omega_k\tau)^{-1}, & \omega_k\tau \rightarrow \infty \end{cases} \quad (25)$$

$$\frac{U_{kk}}{2D_0} \sim \begin{cases} \frac{1}{1+\zeta} + A_{k1}^{\infty} \frac{\sqrt{2}[\sqrt{1+\zeta}-1]}{(1+\zeta)^2}(\omega_k\tau)^{\frac{1}{2}} + O(\omega_k\tau)^{\frac{3}{2}}, & \omega_k\tau \rightarrow 0 \\ 1 - A_{k1}^0 \frac{\zeta}{\sqrt{2}}(\omega_k\tau)^{-\frac{1}{2}} + O(\omega_k\tau)^{-\frac{3}{2}}, & \omega_k\tau \rightarrow \infty \end{cases} \quad (26)$$

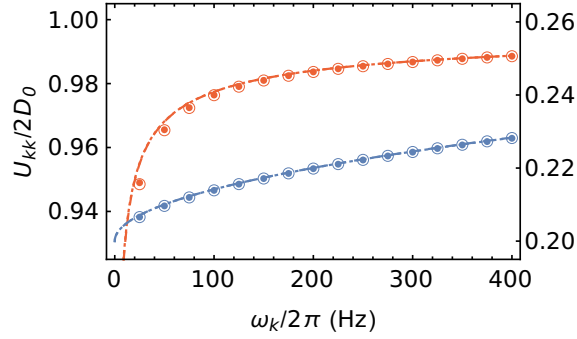
Figure 1 compares the asymptotic behaviour of U_{kk} with that of $u_2(\omega)$ for each of Models 1–3. The upper (dark orange) data corresponds to the system being in the high-frequency regime (i.e. $\omega\tau$ or $\omega_k\tau \rightarrow \infty$), while the lower (blue) data corresponds to the system being in the low-frequency regime (i.e. $\omega\tau$ or $\omega_k\tau \rightarrow 0$). For Model 1, comparison of Eqs. (18) & (20) finds that in the low-frequency limit U_{kk} has the same asymptotic behaviour as $u_2(\omega)$ up to $O(\omega_k\tau)^2$, which is evident in Fig. 1a, but after that there is an $O(\omega_k\tau)^3$ term that does not occur for $u_2(\omega)$. In the high-frequency limit, the coefficient of the $O(\omega_k\tau)^{-2}$ term differs from that of $u_2(\omega)$, and the high-frequency plots of $u_2(\omega)$ and U_{kk} in Fig. 1a reflect this difference. The $O(\omega_k\tau)^{\pm 3}$ terms in Eq. (20) originate from the leading terms in $I_{kk}^R(\beta)$.

For Models 2 & 3, the coefficients of powers of $\omega_k\tau$ in Eqs. (23) & (26) are presented in a way that allows differences in the asymptotic behaviour of U_{kk} and $u_2(\omega)$ to be quickly identified. For both models the difference is characterised by the coefficients A_{k1}^{∞} (in the low-frequency limit) and A_{k1}^0 (in the high-frequency limit). Clearly, the further A_{k1}^{∞} and A_{k1}^0 are from unity the more the asymptotic behaviour of U_{kk} deviates from that of $u_2(\omega)$. Figure 2a shows that A_{k1}^{∞} and A_{k1}^0 differ from 1 most when $k = 1$, but thereafter both approach 1 as $1/k$, the former from below and the latter from above, for increasing k . Neither Eq. (23) nor Eq. (26) contains a term originating from $I_{kk}^R(\beta)$. Looking at the simulated data in Fig. 1b–c, the asymptotic approximations to $u_2(\omega)$ and U_{kk} appear indistinguishable from the exact curves even on the magnified scales used.

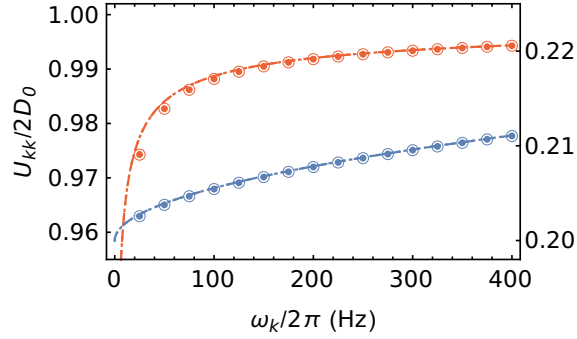
Figure 3 illustrates the asymptotic behaviour of U_{k0} for all three models. The asymptotic approximations in the low-frequency regime are almost indistinguishable from the exact values of U_{k0} , while those in the high-frequency regime have a clear offset, indicating that the next lowest order term in the expansions is important at the selected scales. Recalling that U_{k0} approaches $2D(T)$ for large k [7], those values have also been drawn on the figure as horizontal dashed lines. Apart from one exception, $2D(T)$ provides a reasonable approximation to the exact values of U_{k0} on the scales shown. The exception is the low-frequency data of Model 1, for which the value of $2D(T)$ is off the chosen scale (Fig. 3a).



(a)



(b)



(c)

Figure 1: Comparison of the exact and asymptotic behaviour of U_{kk} with that of $u_2(\omega)$ on magnified scales for Models 1–3. In all parts of the figure the dark-orange data correspond to the high-frequency regime and the left vertical axis, while the blue data correspond to the low-frequency regime and the right vertical axis. Dotted lines denote the exact value of $u_2(\omega)$ for each model, while dashed lines are the corresponding asymptotic approximations presented in Eqs. (18), (21) & (24). In most cases the dotted and dashed lines overlap. Filled circles represent the exact value of U_{kk} , with open circles illustrating the asymptotic approximations of Eqs. (20), (23) & (26). (a) Model 1 with $\eta = 0.8$ and $T/\tau = 0.4$ (dark-orange) and 400 (blue). (b) Model 2 with $\zeta = 0.8$ and $T/\tau = 0.04$ (dark-orange) and 40000 (blue). (c) Model 3 with $\zeta = 4$ and $T/\tau = 0.0004$ (dark-orange) and 400 (blue).

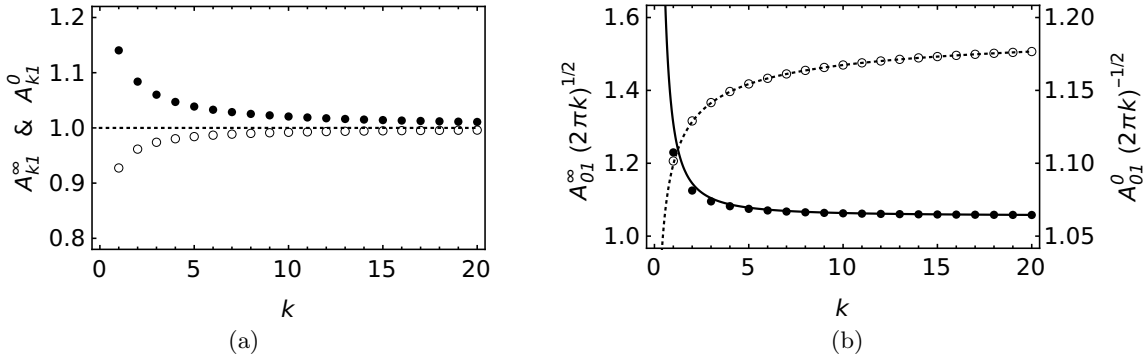


Figure 2: (a) Plots of A_{k1}^{∞} (open circles) and A_{k1}^0 (closed circles) as a function of k . The largest deviation from unity occurs for $k = 1$ ($A_{11}^{\infty} \approx 0.93$ and $A_{11}^0 \approx 1.14$), and thereafter both coefficients approach 1 as k^{-1} for increasing k . (b) Plots of $A_{01}^{\infty} \varpi_k^{1/2}$ (open circles) and $A_{01}^0 \varpi_k^{-1/2}$ (closed circles) as a function of k . The lines represent the asymptotic behaviour of the coefficients as $k \rightarrow \infty$: $A_{01}^{\infty} \varpi_k^{1/2} \sim 2\sqrt{2/\pi} - \varpi_k^{-1/2}$ (dotted) and $A_{01}^0 \varpi_k^{-1/2} \sim (4/3)\sqrt{2/\pi} + \varpi_k^{-3/2}$ (solid).

Consistent with the discussion on the qualitative behaviour of U_{k0} in Sec. 3.2 of [7], the leading terms of Eqs. (19), (22) & (25) are equal to $2D_{\infty}$ and $2D_0$ in the low-frequency and high-frequency limits, respectively. For Model 1, $M[h_{k0}; s] = 0$ for $s = 3, 5, 7, \dots$ so the asymptotic behaviour of U_{k0} in the low-frequency regime stems from $I_{k0}^R(\beta)$ alone. In the high-frequency regime the leading term of $I_{k0}^R(\beta)$ dominates the second term in $I_{k0}^P(\beta)$ so $U_{k0}/2D_0$ approaches 1 as $(\omega_k \tau)^{-1}$ rather than $(\omega_k \tau)^{-2}$. For Models 2 & 3, the coefficients A_{01}^{∞} and A_{01}^0 have been used in Eqs. (22) & (25) to put the asymptotic behaviour of U_{k0} in a form similar to that of $u_2(\omega)$. Even though A_{01}^{∞} diverges and A_{01}^0 tends to zero for increasing k , the products $A_{01}^{\infty} \varpi_k^{1/2}$ and $A_{01}^0 \varpi_k^{-1/2}$, where the factors of $\varpi_k^{\pm 1/2}$ come from $(\omega_k \tau)^{\pm 1/2}$, approach constant values so the corresponding terms remain finite overall (Fig. 2b). Only the $O(\omega_k \tau)^{-1}$ term in the high-frequency regime of Eqs. (22) & (25) originates from $I_{kk}^R(\beta)$.

It is no coincidence that the coefficients A_{k1}^{∞} , A_{k1}^0 , A_{01}^{∞} and A_{01}^0 occur in the asymptotic expansions for both Models 2 & 3. The same thing will happen for any two models having the same powers of $\omega \tau$ in the expansions of $u_2(\omega)$.

4. Structural universality

The aim here is to derive the asymptotic behaviour of U_{k0} & U_{kk} given only the information in Eq. (5). After first introducing an unspecified time-scale parameter τ so that the problem may be written in the dimensionless form of Eq. (6), the MTM can be used to deduce the most significant terms in the asymptotic expansions of U_{k0} & U_{kk} . The details of this laborious process have been included in the Supporting Material (Sec. S-6).

4.1. High-frequency limit

In this limit the known terms of $I_{kl}^P(\beta)$ dominate the leading term of $I_{kl}^R(\beta)$ so that the asymptotic behaviour may be summarised as

$$U_{kl} \sim 2D_0 - C_{l1}^0(k) \omega_k^{-1/2}, \quad \omega_k \tau \rightarrow \infty \quad (27)$$

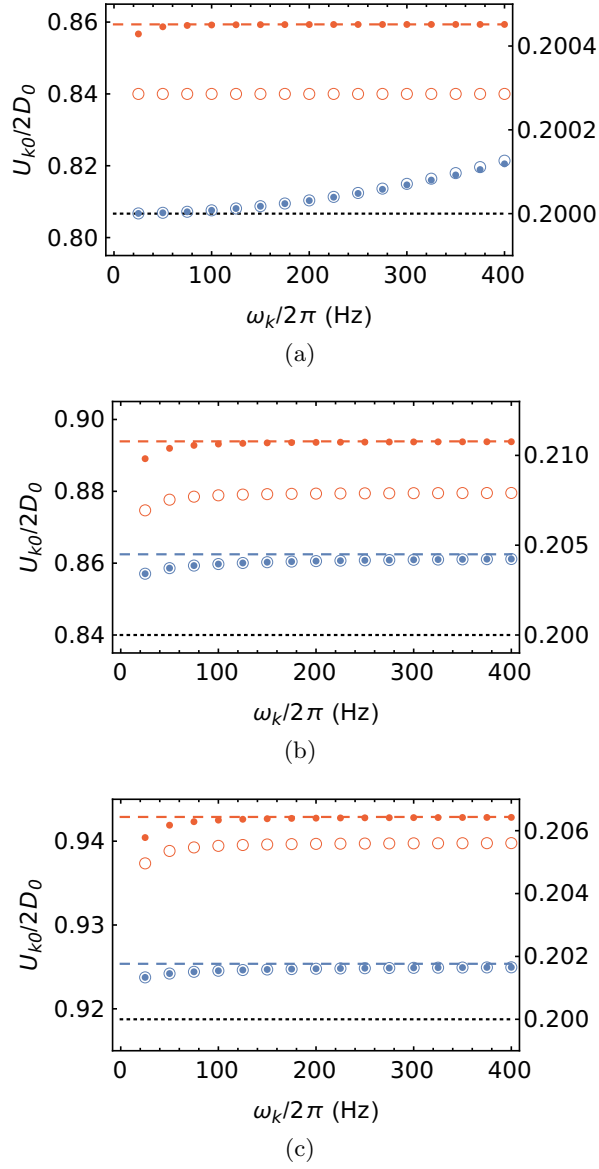


Figure 3: Demonstration of the exact and asymptotic behaviour of U_{k0} for Models 1–3. In all parts of the figure the dark-orange data correspond to the high-frequency regime and the left vertical axis, while the blue data correspond to the low-frequency regime and the right vertical axis. Filled circles represent the exact value of U_{k0} , with open circles illustrating the asymptotic approximations of Eqs. (19), (22) & (25). The black dotted horizontal line is D_∞/D_0 , and the dashed lines are equal to $D(T)/D_0$ for the corresponding value of T/τ . (a) Model 1 with $\eta = 0.8$ and $T/\tau = 0.4$ (dark-orange) and 400 (blue). There is no dashed blue line for this part because $D(T)/D_0 \approx 0.202$, which is off the scale for the low-frequency regime data. (b) Model 2 with $\zeta = 0.8$ and $T/\tau = 0.04$ (dark-orange) and 40000 (blue). (c) Model 3 with $\zeta = 4$ and $T/\tau = 0.0004$ (dark-orange) and 400 (blue).

where $C_{l1}^0(k)/c_0 = A_{l1}^0$. The coefficients, $C_{01}^0(k)$ & $C_{k1}^0(k)$, are respectively proportional to c_0 via the same factors, A_{01}^0 & A_{k1}^0 , that appeared in the results for Models 2 & 3. This was expected because those models were constructed in [6] with the universal high-frequency behaviour built in. For Models 2 & 3 the constant c_0 equates to $\sqrt{2}\zeta\tau^{-1/2}D_0$ so that $S/V \equiv \zeta d/\sqrt{\tau D_0}$. The high-frequency behaviour of Model 1 is not consistent with the predicted universality relation in Eq. (5), so there is no S/V equivalent for that model.

Although Eq. (27) has been presented with the same qualitative dependence on frequency as $u_2(\omega)$, it should be remembered that the true asymptotic variable is β . The k -dependence of $C_{01}^0(k)$ & $C_{k1}^0(k)$ therefore complicates the interpretation of U_{kk} & U_{k0} . For example, even though U_{kk} eventually approaches $2D_0$ as $\omega_k^{-1/2}$ because $A_{k1}^0 \sim 1$ for large k (re Fig. 2a), plots of U_{kk} versus ω_k may show substantial deviation from that behaviour for the low values of k accessible with OGSE-DWI. On the other hand, $A_{01}^0 \varpi_k^{-1/2} \sim (4/3)\sqrt{2/\pi} + \varpi_k^{-3/2}$ for large k (re Fig. 2b), so, rather than varying as $\omega_k^{-1/2}$, plots of U_{k0} against ω_k will quickly approach a constant value that is consistent with the result $\lim_{k \rightarrow \infty} U_{k0} = 2D(T)$ proved in [7].

4.2. Low-frequency limit

The qualitative behaviour in the low-frequency limit depends on the value of ϑ . For $\vartheta > 0$ there are three separate cases:

- (a) $0 < \vartheta < 3$. In this case the leading $O(\beta^{-\vartheta-1})$ term of $I_{kl}^P(\beta)$ dominates the $O(\beta^{-4})$ term of $I_{kl}^R(\beta)$. Accordingly, the latter term is ignored and the asymptotic behaviour of U_{kk} & U_{k0} is

$$U_{kl} \sim 2D_\infty + C_{l1}^\infty(k, \vartheta) \omega_k^\vartheta, \quad \omega_k \tau \rightarrow 0 \quad (28)$$

with $C_{l1}^\infty(k, \vartheta)/c_\infty = B_{kl}M[h_{kl}; \vartheta + 1]/\varpi_k^\vartheta$.

- (b) $\vartheta = 3$. This is a special case where, since the pole at $\vartheta + 1 = 4$ of $M[f_1; 1 - s]$ coincides with the first pole of $M[h_{kl}; s]$, $G_{l1}(s)$ has a second order pole. As a consequence, the leading term of $I_{kl}^Q(\beta)$ dominates everything except the leading $O(\beta^{-1})$ term of $I_{kl}^P(\beta)$. The asymptotic behaviour of the observed quantities is therefore distinguished by a logarithmic dependence on frequency

$$U_{kl} \sim 2D_\infty - C_{l2}^\infty(k) \omega_k^3 \ln \omega_k \tau, \quad \omega_k \tau \rightarrow 0 \quad (29)$$

where $C_{l2}^\infty(k)/c_\infty = B_{kl}/\varpi_k^3$.

- (c) $\vartheta > 3$. This case is the reverse of the $0 < \vartheta < 3$ case as the $O(\beta^{-\vartheta-1})$ term of $I_{kl}^P(\beta)$ is now subdominant to the $O(\beta^{-4})$ term of $I_{kl}^R(\beta)$. The qualitative behaviour of U_{kk} & U_{k0} therefore differs from that of $u_2(\omega)$:

$$U_{kl} \sim 2D_\infty + C_{l3}^\infty(k) \omega_k^3, \quad \omega_k \tau \rightarrow 0 \quad (30)$$

where $C_{l3}^\infty(k)/2D_0 = B_{kl}\tau^3 M[f; -3]/\varpi_k^3$. Clearly, for systems of this type the global information associated with ϑ is obfuscated by an $O(\omega_k^3)$ term.

Details on how $M[h_{kl}; \vartheta + 1]$ may be evaluated can be found in Sec. S-3 of the Supporting Material, while Sec. S-7 considers the behaviour of $C_{l1}^\infty(k, \vartheta)/c_\infty$ with respect to ϑ and k . From that information it can be shown that for large k ,

$$C_{k1}^\infty(k, \vartheta) \omega_k^\vartheta \sim O(k^\vartheta)$$

and

$$C_{01}^{\infty}(k, \vartheta) \omega_k^{\vartheta} \sim \begin{cases} O(1), & 0 < \vartheta < 1 \\ O(\ln k), & \vartheta = 1 \\ O(k^{\vartheta-1}), & \vartheta > 1. \end{cases}$$

That is, the apparent frequency-dependence of U_{kk} when plotted against ω_k will approach the frequency-dependence of $u_2(\omega)$, while the apparent frequency-dependence of U_{k0} will never match the frequency-dependence of the spectral density.

5. Discussion

The MTM has been introduced as a general technique that can be applied to derive the asymptotic behaviour of U_{kk} & U_{k0} in both the low and high frequency limits. Exact forms for U_{kk} & U_{k0} for Models 1 & 2 were calculated previously in [7], and expansion of those results verifies the results of the MTM when applied to those models. The advantage of the MTM is that it can be used even when the exact forms of U_{kk} & U_{k0} are difficult to evaluate, as was the case for Model 3, or when the precise form of $u_2(\omega)$ is unknown, as was true in Sec. 4.

5.1. Apparent diffusion coefficient

Given the popularity of the apparent diffusion coefficient (ADC) signal model for the interpretation of DWI data, it is pertinent to also mention the asymptotic behaviour of the ADC. A relationship between the ADC for a single-harmonic MPG (i.e. Eq. (1)), and U_{kk} & U_{k0} was presented as Eq. (27) in [7]. Inserting Eq. (27) into that relationship in the appropriate way, the asymptotic behaviour in the high-frequency limit is

$$\text{ADC}_k(\phi) \sim D_0 - C_0(k, \phi) \omega_k^{-1/2}, \quad (31)$$

with $C_0(k, \phi)/c_0 = (A_{k1}^0 + 2A_{01}^0 \sin^2 \phi)/(2 + 4 \sin^2 \phi)$.

An expression for the universal high-frequency behaviour of the ADC was previously derived in [10]. Also, although the ADC is not specifically mentioned, the high-frequency behaviour of the signal observed using an oscillating MPG was discussed in an appendix of [11]. After a suitable translation between the notations used in [10] & [11] and that used here, it is found that the results presented in those studies are equivalent to Eq. (31). In particular, the quantities $c'(\varphi, N)$ (in Eq. (14) of [10]) and $\tilde{c}(\varphi, N)/\sqrt{2}$ (in Eq. (C6) of [11]) are equivalent to $\sqrt{2}C_0(k, \phi)/c_0$. More details of the comparison may be found in the Supporting Material (Sec. S-8).

An asymptotic expansion for the ADC in the low-frequency limit could be derived by inserting Eqs. (28)–(30) into the aforementioned relationship, but that procedure is complicated by the dependence on ϑ . A more straightforward approach using the MTM is presented in Sec. S-9 of the Supporting Material. For $\phi = 0$ the resulting expansion is equivalent to that for $U_{kk}/2$ (re Sec. 4.2) as expected. For the other extreme when $\phi = \pi/2$, the result may be summarised as

$$\text{ADC}_k(\pi/2) \sim \begin{cases} D_{\infty} + C_1^{\infty}(k, \pi/2, \vartheta) \omega_k^{\vartheta}, & 0 < \vartheta < 5 \\ D_{\infty} - C_2^{\infty}(k, \pi/2) \omega_k^5 \ln \omega_k \tau, & \vartheta = 5 \\ D_{\infty} + C_3^{\infty}(k, \pi/2) \omega_k^5, & \vartheta > 5 \end{cases} \quad (32)$$

where $C_1^{\infty}(k, \pi/2, \vartheta)/c_{\infty} = 2\varpi_k^{2-\vartheta}(M[h_{kk}; \vartheta + 1] - M[h_{k0}; \vartheta + 1])/3\pi$, $C_2^{\infty}(k, \pi/2)/c_{\infty} = 1/3\pi^2 k$ and $C_3^{\infty}(k, \pi/2)/D_0 = M[f; -5]\tau^5/3\pi^2 k$. Sec. S-9 also considers the behaviour of $C_1^{\infty}(k, \pi/2, \vartheta)$ with respect to ϑ and k .

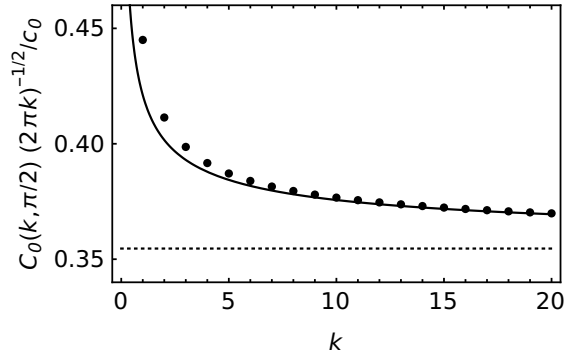


Figure 4: Plot of $C_0(k, \pi/2) \varpi_k^{-1/2}/c_0$ as a function of k . The solid line represents the asymptotic behaviour $C_0(k, \pi/2) \varpi_k^{-1/2}/c_0 \sim (4/9)\sqrt{2/\pi} + 1/6\varpi_k^{1/2}$ for large k , while the dotted line is the limit $(4/9)\sqrt{2/\pi}$ as $k \rightarrow \infty$.

5.2. OGSE-DWI in practice

This study has concentrated on a form of OGSE-DWI where the applied MPG is a pure single-harmonic waveform (i.e. Eq. (1)). Unfortunately, the only way that a single-harmonic MPG can be implemented in practice is when $\phi = \pi/2$, which implies that precise independent measurements of U_{kk} & U_{k0} are impractical. The only quantity that can actually be measured with *pure* OGSE-DWI is $\text{ADC}_k(\pi/2)$. Nevertheless, assuming that the range of accessible frequencies ($\approx 10^1$ – 10^3 Hz) falls in either the high- or low-frequency regime for a given system, measurements of $\text{ADC}_k(\pi/2)$ can be used to extract structural information in certain situations. In the high-frequency limit, the k -dependence of $C_0(k, \pi/2)$ in Eq. (31) means that a slightly more subtle analysis is required than simply fitting for a constant coefficient of $\omega_k^{-1/2}$. $C_0(k, \pi/2)$ combines the characteristics of both A_{k1}^0 and A_{01}^0 (re Fig. 2), so that $C_0(k, \pi/2) \varpi_k^{-1/2}/c_0 \sim (4/9)\sqrt{2/\pi} + 1/6\varpi_k^{1/2}$ for large k (Fig. 4). That is, measurements of the ADC will gradually approach a constant value as $k^{-1/2}$, and so independent estimates of D_0 and c_0 (and hence S/V) may be possible if sufficient signal-to-noise is available.

The situation in the low-frequency limit is more complicated due to the added dependence on ϑ . An analysis of the behaviour of the coefficient $C_1^\infty(k, \pi/2, \vartheta)$ in Eq. (32) (see Supporting Material, Sec. S-9) finds that for large k and $\vartheta > 0$,

$$C_1^\infty(k, \pi/2, \vartheta) \omega_k^\vartheta \sim O(k^\vartheta). \quad (33)$$

So, in the low-frequency limit the apparent frequency-dependence of $\text{ADC}_k(\pi/2)$ when plotted against ω_k will tend towards that of the spectral density when $0 < \vartheta < 5$, and hence it is likely that structural information can be extracted from the data for samples falling into that range of ϑ . On the other hand, Eq. (32) indicates that the $O(\omega_k^\vartheta)$ term will always be subdominant to, and hence obfuscated by, an $O(\omega_k^5)$ term when $\vartheta > 5$. It is also unlikely that the logarithmic dependence on frequency corresponding to the special case $\vartheta = 5$ can be clearly identified within the narrow range of frequencies accessible with OGSE-DWI. Using pure OGSE-DWI to characterise the structural organisation of a material with a dynamic exponent falling outside of the range $0 < \vartheta < 5$ may be challenging.

It was suggested in [7] that OGSE-DWI experiments be performed by varying k while keeping T constant at its longest possible value, but such a protocol is not essential. The same results would apply for the asymptotics of the ADC if the experiments were performed after first setting k and

then varying T , or even if some hybrid protocol were used where both k and T are systematically varied. Even though the limits on the spectral range will remain unaltered, using an acquisition protocol where T is varied has the potential benefit of improved spectral resolution. Making acquisitions for multiple values of T might also aid in the estimation of ϑ . Rather than being a simple fit of $\text{ADC}_k(\pi/2)$ against a single frequency variable, the estimation problem requires that data is fitted against the two independent variables k and T . Whatever protocol is adopted for the lab, it is important to remember the k and T dependence of the data in the analysis.

Instead of a pure single-harmonic MPG, OGSE-DWI is commonly performed using some type of approximation to a sinusoidal waveform (e.g. [4, 5]), or at least a waveform that has the symmetry $g(t) = g(T-t)$ (e.g. [2, 3]). As previously noted in [7], any such waveform will contain contributions from multiple harmonics so the precise signal equation will be more complicated than the specialised case in Eq. (2). More important to accurate quantification of complex microstructures, it is unclear how well the expansions derived for U_{kk} in this study will hold as approximations to the asymptotic behaviour of the signal when observed with a multiharmonic MPG. The effects and potential errors associated with multiharmonic MPGs will be investigated in a forthcoming article.

6. Conclusions

The goal of this study was to investigate how the global features associated with the universality relations in Eq. (5) emerge in the asymptotic behaviour of OGSE-DWI signal. The MTM was introduced as a technique to achieve that goal without having to first evaluate exact forms for U_{kk} & U_{k0} . Given that the limitations on T and k restrict the range of frequencies accessible to OGSE-DWI, it is the value of T relative to the time-scale τ characterising the response of the system that actually determines whether the condition for observations in either asymptotic regime is met or not. In the high-frequency limit, although U_{kk} & U_{k0} have the same qualitative dependence on frequency as $u_2(\omega)$, the k -dependence of the coefficients complicates the interpretation. In the low-frequency limit, the asymptotic behaviour of U_{kk} & U_{k0} is further complicated by the dependence on ϑ . In some circumstances the true asymptotic behaviour of the system may be obscured by the characteristics of the filters $H_{kl}(\omega; T)$.

Asymptotic expansions were also derived for the ADC associated with a single-harmonic MPG. The expression for the high-frequency limit was found to be equivalent to the results presented in two earlier studies. Unfortunately, it is not possible to make specific independent measurements of U_{kk} & U_{k0} in practice due to the difficulty associated with implementing a pure sinusoidal MPG. This means that the only quantity that can be measured with a single-harmonic MPG is $\text{ADC}_k(\pi/2)$. Nevertheless, measurements of $\text{ADC}_k(\pi/2)$ can be used to estimate S/V when the window of frequencies accessible with OGSE-DWI lies in the high-frequency regime for a particular sample. Estimates of ϑ in the low-frequency limit might also be possible for materials with $0 < \vartheta < 5$, but outside of that range producing reliable estimates may be challenging. In any case, the estimation procedure requires that the data is fitted against both k and T rather than a single frequency variable. Methods to analyse the effects of multiharmonic MPGs will be addressed in a future article.

References

- [1] J. Stepisnik, “Analysis of NMR self-diffusion measurements by a density matrix calculation,” *Physica B*, vol. 104, pp. 350–364, 1981, 10.1016/0378-4363(81)90182-0.

- [2] P. T. Callaghan, J. Stepisnik, “Frequency-domain analysis of spin motion using modulated-gradient NMR,” *J. Magn. Reson. A*, vol. 117, pp. 118–122, 1995, 10.1006/jmra.1995.9959.
- [3] P. T. Callaghan, J. Stepisnik, “Generalized analysis of motion using magnetic field gradients,” *Adv. Magn. Opt. Reson.*, vol. 19, pp. 325–388, 1996, 10.1016/S1057-2732(96)80020-9.
- [4] E. C. Parsons, M. D. Does, J. C. Gore, “Modified oscillating gradient pulses for direct sampling of the diffusion spectrum suitable for imaging sequences,” *Magn. Reson. Imaging*, vol. 21, pp. 279–285, 2003, 10.1016/S0730-725X(03)00155-3.
- [5] M. D. Does, E. C. Parsons, J. C. Gore, “Oscillating gradient measurements of water diffusion in normal and globally ischemic rat brain,” *Magn. Reson. Med.*, vol. 49, pp. 206–215, 2003, 10.1002/mrm.10385.
- [6] D. S. Novikov, V. G. Kiselev, “Surface-to-volume ratio with oscillating gradients,” *J. Magn. Reson.*, vol. 210, pp. 141–145, 2011, 10.1016/j.jmr.2011.02.011.
- [7] J. Kershaw, T. Obata, “Oscillating-gradient spin-echo diffusion-weighted imaging (OGSE-DWI) with a limited number of oscillations: I. Signal equation,” *J. Magn. Reson.*, vol. 326, pp. 106962, 2021, 10.1016/j.jmr.2021.106962.
- [8] D. S. Novikov, J. H. Jensen, J. A. Helpert, E. Fieremans, “Revealing mesoscopic structural universality with diffusion,” *Proc. Nat. Acad. Sci.*, vol. 111, pp. 5088–5093, 2014, 10.1073/pnas.1316944111.
- [9] N. Bleistein, R. A. Handelsman, *Asymptotic expansions of integrals*. New York, NY, USA: Holt, Rinehart and Winston, 1975.
- [10] A. L. Sukstanskii, “Exact analytical results for ADC with oscillating diffusion sensitizing gradients,” *J. Magn. Reson.*, vol. 234, pp. 135–140, 2013, 10.1016/j.jmr.2013.06.016.
- [11] D. S. Novikov, E. Fieremans, S. N. Jespersen, V. G. Kiselev, “Quantifying brain microstructure with diffusion MRI: Theory and parameter estimation,” *NMR Biomed.*, vol. 32, pp. e3998, 2019, 10.1002/nbm.3998.

List of Symbols

| Symbol | Definition | First use |
|-------------------------------|---|-----------|
| A_{01}^∞, A_{01}^0 | k -dependent coefficients present in the expansions of U_{k0} for Models 2 & 3 | Eq. (22) |
| A_{k1}^∞, A_{k1}^0 | k -dependent coefficients present in the expansions of U_{kk} for Models 2 & 3 | Eq. (23) |
| $\text{ADC}_k(\phi)$ | apparent diffusion coefficient for a single-harmonic MPG of frequency ω_k and phase ϕ | Eq. (31) |
| a_{lj} | lower limit of the analytic strip of $G_{lj}(s)$ | Sec. 2.2 |
| a_{sk}, a_{ck} | symbols used for convenience in Models 2 & 3 | Eq. (22) |
| B_{kl} | constant used in the definition of $H_{kl}(\omega; T)$ | Eq. (4) |
| b_{lj} | upper limit of the analytic strip of $G_{lj}(s)$ | Sec. 2.2 |
| β | ratio of T to τ | Sec. 2.1 |
| $C(z)$ | Fresnel cosine integral | Sec. 3 |
| $C_{l1}^0(k)$ | coefficient in the high-frequency universal behaviour of U_{kl} | Eq. (27) |
| $C_{l1}^\infty(k, \vartheta)$ | coefficients in the low-frequency universal behaviour of U_{kl} | Eq. (28) |
| $C_{l2}^\infty(k)$ | | Eq. (29) |
| $C_{l3}^\infty(k)$ | | Eq. (30) |
| $C_0(k, \phi)$ | coefficient in the high-frequency universal behaviour of $\text{ADC}_k(\phi)$ | Eq. (31) |
| $C_1^\infty(k, \vartheta)$ | coefficients in the low-frequency universal behaviour of $\text{ADC}_k(\phi)$ | Eq. (32) |
| $C_2^\infty(k)$ | | |
| $C_3^\infty(k)$ | | |
| c_0, c_∞ | coefficients characterising the universal asymptotic behaviour of the spectral density | Eq. (5) |
| D_0, D_∞ | diffusion coefficients associated with the asymptotic limits of the spectral density | Eq. (5) |
| $D(T)$ | cumulative diffusion coefficient at time T | Sec. 1 |
| d | spatial dimension | Eq. (5) |
| $\delta_{n,m}$ | Kronecker delta | Eq. (1) |
| η | parameter used in Model 1 to represent disorder strength | Eq. (18) |
| G | amplitude of the MPG | Sec. 1 |
| $G_{lj}(s)$ | product of $M[f_j; 1 - s]$ and $M[h_{kl}; s]$ | Sec. 2.2 |
| $f(v)$ | dimensionless form of $u_2(\omega)$ | Eq. (6) |
| $f_j(v)$ | partitions of $f(v)$, $j = 1, 2$ | Eq. (7) |
| f_n^0, f_n^∞ | n th coefficients in the expansions of $f(v)$ | Eq. (12) |
| $g(t)$ | MPG waveform | Eq. (1) |
| γ | gyromagnetic ratio of the proton | Eq. (2) |
| $H_{kl}(\omega; T)$ | kernel in the integral relationship between U_{kl} and $u_2(\omega)$ | Eq. (3) |
| $h_{kl}(v)$ | dimensionless form of $H_{kl}(\omega; T)$ | Eq. (6) |
| h_{ln}^0, h_{ln}^∞ | n th coefficients in the expansions of $h_{kl}(v)$ | Eq. (10) |
| $I_{kl}(\beta)$ | dimensionless form of U_{kl} | Eq. (6) |
| $I_{kl}^j(\beta)$ | partition of $I_{kl}(\beta)$ associated with $f_j(v)$ | Eq. (9) |
| $I_{kl}^P(\beta)$ | partition of $I_{kl}(\beta)$ associated with the set P_{lj} | Eq. (15) |
| $I_{kl}^Q(\beta)$ | partition of $I_{kl}(\beta)$ associated with the set Q_{lj} | Eq. (17) |
| $I_{kl}^R(\beta)$ | partition of $I_{kl}(\beta)$ associated with the set R_{lj} | Eq. (16) |

| | | |
|----------------------------|--|----------|
| K_{lpr}^j | quantity associated with the residue of the second order poles in the sets Q_{lj} , $j = 1, 2$ | Eq. (17) |
| k | number of oscillations in the selected MPG | Eq. (1) |
| l | equals either 0 or k | Eq. (3) |
| $M[f; s]$ | Mellin transform of $f(v)$ | Sec. 2.2 |
| $M[f_j; s]$ | Mellin transform of $f_j(v)$, $j = 1, 2$ | Sec. 2.2 |
| $M[h_{kl}; s]$ | Mellin transform of $h_{kl}(v)$ | Sec. 2.2 |
| ω | angular frequency | Eq. (3) |
| ω_k | angular frequency of the selected MPG | Eq. (1) |
| P_{lj} | sets containing non-negative integers p , $j = 1, 2$ | Sec. 2.3 |
| p | non-negative integer indexing the poles of $G_{lj}(s)$ | Sec. 2.3 |
| p | structural exponent | Eq. (5) |
| ϕ | phase of the selected MPG | Eq. (1) |
| ϖ_k | $= 2\pi k$ | Eq. (4) |
| Q_{lj} | sets containing non-negative integer pairs (p, q) , $j = 1, 2$ | Sec. 2.3 |
| R_{lj} | sets containing non-negative integers r , $j = 1, 2$ | Sec. 2.3 |
| r | non-negative integer indexing the poles of $G_{lj}(s)$ | Sec. 2.3 |
| S/V | surface-to-volume ratio | Eq. (5) |
| $S(z)$ | Fresnel sine integral | Sec. 3 |
| s | arbitrary complex variable | Sec. 2.2 |
| s_n | n th pole of $G_{lj}(s)$ | Sec. 2.2 |
| $s_k(T)$ | signal for single-harmonic MPG of frequency ω_k | Eq. (2) |
| T | duration of a MPG | Eq. (1) |
| t | time variable | Sec. 1 |
| τ | correlation time | Sec. 2.1 |
| ϑ | dynamical exponent | Eq. (5) |
| θ_{1n}, θ_{2n} | n th powers of v in the expansions of $f(v)$ | Eq. (12) |
| U_{kl} | $l = 0$ or k ; quantities in the signal equation for a single harmonic MPG | Eq. (2) |
| $u_2(\omega)$ | spectral density of molecular diffusion | Sec. 1 |
| v | dimensionless variable equal to $\omega\tau$ | Eq. (6) |
| v_0 | arbitrary positive real number | Eq. (7) |
| ζ | parameter related to the volume fraction occupied by permeable membranes in Models 2 & 3 | Eq. (22) |

Supporting Material

This document contains material supporting the results presented in the manuscript “Oscillating-gradient spin-echo diffusion-weighted imaging (OGSE-DWI) with a limited number of oscillations: II. Asymptotics” by Jeff Kershaw & Takayuki Obata.

Section, equation, figure and table numbers local to this supporting material are prefaced by an “S”. All other numbering refers to items in the main text.

Table of contents

| | | |
|-------------|---|-----------|
| <i>S-1</i> | <i>Asymptotic expansion of integrals using the Mellin transform method</i> | <i>1</i> |
| <i>S-2</i> | <i>Generalised methods for Mellin transforms</i> | <i>5</i> |
| <i>S-3</i> | <i>Some details on the Mellin transforms of $h_{k0}(v)$ & $h_{kk}(v)$</i> | <i>8</i> |
| <i>S-4</i> | <i>Some details on the asymptotic expansion of U_{k0} & U_{kk} for Models 1 & 2</i> | <i>9</i> |
| <i>S-5</i> | <i>Asymptotic expansion of U_{k0} & U_{kk} for Model 3</i> | <i>13</i> |
| <i>S-6</i> | <i>Structural universality</i> | <i>17</i> |
| <i>S-7</i> | <i>Behaviour of $C_{k1}^\infty(k, \vartheta)$ & $C_{01}^\infty(k, \vartheta)$</i> | <i>21</i> |
| <i>S-8</i> | <i>Some comments on two previous derivations of the ADC</i> | <i>22</i> |
| <i>S-9</i> | <i>Low-frequency asymptotic behaviour of the ADC</i> | <i>27</i> |
| <i>S-10</i> | <i>Various integrals</i> | <i>29</i> |

S-1. Asymptotic expansion of integrals using the Mellin transform method

Let $a, b \in \mathbb{R}$ and let $h(x)$ be a locally integrable function¹ on $(0, \infty)$ such that $h(x) \sim O(x^{-a})$ as $x \rightarrow 0$ and $h(x) \sim O(x^{-b})$ as $x \rightarrow \infty$. Then, if $a < b$ and $s \in \mathbb{C}$, the *Mellin transform* of $h(x)$ is defined as

$$M[h; s] = \int_0^\infty dx x^{s-1} h(x), \quad (\text{S.1})$$

which is analytic in the infinite strip $a < \text{Re } s < b$ parallel to the imaginary axis. The corresponding inversion formula is

$$h(x) = \frac{1}{2\pi i} \int_{r-i\infty}^{r+i\infty} ds x^{-s} M[h; s] \quad (\text{S.2})$$

with r being a real number such that $a < r < b$. Also, note that by making a simple change of variables in Eq. (S.1) it can be shown for real $\lambda > 0$ that

$$M[h(\lambda x); s] = \lambda^{-s} M[h; s]. \quad (\text{S.3})$$

Even though Eq. (S.1) only defines $M[h; s]$ for the analytic strip $a < \text{Re } s < b$, it is a useful property of the Mellin transform that it can be analytically continued to a meromorphic function throughout the whole complex plane [9]. Moreover, the behaviour of $M[h; s]$ near the poles can be predicted from the asymptotic behaviour of $h(x)$. Specifically, if

$$h(x) \sim \sum_{n=0}^{\infty} \sum_{m=0}^{M_n^0} h_{nm}^0 (\ln x)^m x^{a_n}, \quad x \rightarrow 0 \quad (\text{S.4})$$

¹A function $h(x)$ is locally integrable on $(0, \infty)$ if $\int_{x_1}^{x_2} dx h(x) < \infty$ for all x_1, x_2 that satisfy $0 < x_1 < x_2 < \infty$.

with $\text{Re } a_n$ being a strictly monotonic increasing sequence of numbers, starting from $\text{Re } a_0 = -a$, and M_n^0 is a finite non-negative integer for each n , then $M[h; s]$ can be continued analytically into the left-hand plane $\text{Re } s < a$ and

$$M[h; s] \sim \sum_{m=0}^{M_n^0} \frac{(-)^m h_{nm}^0 m!}{(s + a_n)^{m+1}}, \quad s \rightarrow -a_n. \quad (\text{S.5})$$

Similarly, if

$$h(x) \sim \sum_{n=0}^{\infty} \sum_{m=0}^{M_n^{\infty}} h_{nm}^{\infty} (\ln x)^m x^{-b_n}, \quad x \rightarrow \infty, \quad (\text{S.6})$$

where $\text{Re } b_n$ is a strictly monotonic increasing sequence of numbers, beginning with $\text{Re } b_0 = b$, and M_n^{∞} is a finite non-negative integer for each n , then $M[h; s]$ can be continued analytically into the right-hand plane $\text{Re } s > b$ with

$$M[h; s] \sim - \sum_{m=0}^{M_n^{\infty}} \frac{(-)^m h_{nm}^{\infty} m!}{(s - b_n)^{m+1}}, \quad s \rightarrow b_n. \quad (\text{S.7})$$

Notice that the poles of $M[h; s]$ in the left-hand (or right-hand) complex plane from the analytic strip correspond to the powers of x in the expansion about 0 (or ∞). Furthermore, the order of the n th pole is determined by the highest power of $\ln x$ in the n th term of the corresponding expansion. If $M_n^0 = M_n^{\infty} = 0 \forall n$ then the poles of $M[h; s]$ are all simple.

There is also an interesting relationship between the Mellin and Fourier transforms. After making the change of variable $y = \ln x$ in Eq. (S.1) it is easy to show that

$$M[h; s] = \int_{-\infty}^{\infty} dy e^{\sigma y} h(e^y) e^{i\nu y} \quad (\text{S.8})$$

where $\sigma = \text{Re } s$. That is, the Mellin transform of $h(x)$ is equal to the Fourier transform of the function $h_{\sigma}(y) = e^{\sigma y} h(e^y)$. This is useful because if $h_{\sigma}(y)$ is integrable on \mathbb{R} , then the Riemann-Lebesgue lemma implies that

$$\lim_{|\nu| \rightarrow \infty} M[h; s] = 0 \quad (\text{S.9})$$

with $\nu = \text{Im } s$. Note that $h_{\sigma}(y)$ will always be integrable for σ within the analytic strip. Similar arguments as those used to analytically continue the Mellin transform can then be used to show that the limit is true $\forall \sigma \in \mathbb{R}$.

Another useful identity for Mellin transforms can be obtained by integrating $z^{s-1} h(z)$ around the sector S shown in Fig. S.1. Here θ_0 is chosen so that the poles and branch points of $h(z)$ are excluded from being either on or inside the boundary of the sector. θ_0 is also selected as positive or negative according to whether ν is positive or negative. When σ is within the analytic strip it is straightforward to show using the asymptotic behaviour of h that the integral along the arc approaches zero as $R \rightarrow \infty$. The following relationship is therefore obtained

$$M[h(x); s] = e^{i\theta_0 s} \int_0^{\infty} dr r^{s-1} h(re^{i\theta_0}) = e^{i\theta_0 s} M[h(re^{i\theta_0}); s]. \quad (\text{S.10})$$

Since the asymptotic behaviour of $h(re^{i\theta_0})$ wrt r is similar to that of $h(x)$ wrt x , all of the preceding results for Mellin transforms can be shown to also apply for $M[h(re^{i\theta_0}); s]$. In particular, it is

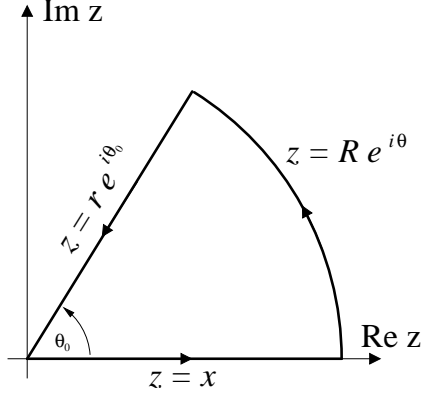


Figure S.1: Contour S used to obtain Eq. (S.10). The contour consists of three lines with the parametrisation for each written next to it. When $\theta_0 < 0$ is chosen the contour is reflected about the $\text{Re } z$ axis to lie in the lower-half plane.

analytic for $a < \sigma < b$, goes to zero as $\nu \rightarrow \infty$ (re Eq. (S.9)) and can be analytically continued into the whole complex plane. This means that

$$|M[h(x); s]| \sim O(e^{-\theta_0 \nu}), \quad |\nu| \rightarrow \infty. \quad (\text{S.11})$$

Analytic continuation guarantees that this behaviour holds $\forall \sigma \in \mathbb{R}$.

The Parseval formula for Mellin transforms is introduced next. Analogous to the case for $h(x)$, let $f(x)$ be another locally integrable function such that

$$f(x) \sim \begin{cases} \sum_{n=0}^{\infty} \sum_{m=0}^{M_n^0} f_{nm}^0 (\ln x)^m x^{c_n}, & x \rightarrow 0 \\ \sum_{n=0}^{\infty} \sum_{m=0}^{M_n^\infty} f_{nm}^\infty (\ln x)^m x^{-d_n}, & x \rightarrow \infty \end{cases} \quad (\text{S.12})$$

with $\text{Re } c_0 = -c$ and $\text{Re } d_0 = d$. Assume also that $c < d$. Together with the previously stated condition that $a < b$, this assumption ensures that the analytic strip $a + c < \text{Re } s < b + d$ of $M[fh; s]$ is always nonempty. Now, using Eqs. (S.1) & (S.2) it is possible to show that ²

$$M[fh; s] = \int_0^\infty dx x^{s-1} f(x)h(x)$$

²To use the inverse transform of $M[h; s]$ the real number r must be within the analytic strip $a < \text{Re } s < b$. On the other hand, the derivation could have been performed using the inverse transform of $M[f; s]$ so that

$$M[fh; s] = \frac{1}{2\pi i} \int_{r'-i\infty}^{r'+i\infty} ds'' M[h; s-s'']M[f; s''] = \frac{1}{2\pi i} \int_{\sigma-r'-i\infty}^{\sigma-r'+i\infty} ds' M[h; s']M[f; s-s'],$$

where r' lies in the analytic strip $c < \text{Re } s < d$ and the change of variable $s' = s - s''$ has been used. For this result to be equal to Eq. (S.13), $\sigma = \text{Re } s$ has to be such that $r = \text{Re } s - r'$. Since $a < r < b$ and $c < r' < d$, this is equivalent to saying that $a + c < \text{Re } s < b + d$, which is the analytic strip of $M[fh; s]$. That is, the two derivations are consistent as long as s lies within the analytic strip of $M[fh; s]$.

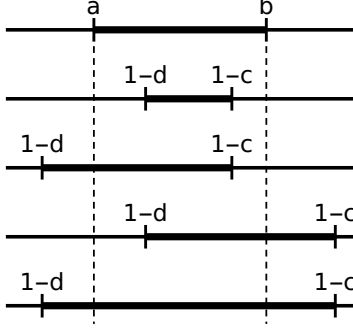


Figure S.2: Intersection between the analytic strips of $M[f; 1-s]$ and $M[h; s]$ for the case $a < b$ and $c < d$. In this case the Mellin transforms of both $f(x)$ and $h(x)$ are defined in the ordinary sense. The upper line represents the analytic strip of $M[h; s]$, while the lower four lines represent the four distinct cases for how the analytic strip of $M[f; 1-s]$ might overlap. All four cases can be summarised as the interval $(\max\{a, 1-d\}, \min\{1-c, b\})$.

$$\begin{aligned}
&= \int_0^\infty dx x^{s-1} f(x) \left\{ \frac{1}{2\pi i} \int_{r-i\infty}^{r+i\infty} ds' x^{-s'} M[h; s'] \right\} \quad (a < r < b) \\
&= \frac{1}{2\pi i} \int_{r-i\infty}^{r+i\infty} ds' M[h; s'] \int_0^\infty dx x^{s-s'-1} f(x) \\
&= \frac{1}{2\pi i} \int_{r-i\infty}^{r+i\infty} ds' M[h; s'] M[f; s-s']. \tag{S.13}
\end{aligned}$$

It is assumed here that the conditions necessary for the interchange of integration order are satisfied. The Parseval formula follows immediately from Eq. (S.13) after setting $s = 1$:

$$\int_0^\infty dx f(x) h(x) = \frac{1}{2\pi i} \int_{r-i\infty}^{r+i\infty} ds M[h; s] M[f; 1-s]. \tag{S.14}$$

Now, using the Parseval formula and Eq. (S.3), it is possible to show for $f(x)$ and $h(x)$ as above that

$$I(\lambda) = \int_0^\infty dx f(x) h(\lambda x) = \frac{1}{2\pi i} \int_{r-i\infty}^{r+i\infty} ds \lambda^{-s} M[f; 1-s] M[h; s], \tag{S.15}$$

where λ is a positive real number. On this occasion it is assumed that r lies within the intersection of the strips of analyticity of $M[h; s]$ (i.e. $a < \text{Re } s < b$) and $M[f; 1-s]$ (i.e. $1-d < \text{Re } s < 1-c$). The intersection will always be nonempty because the conditions for the left-hand side of Eq. (S.15) to converge are

$$a + c < 1 \quad \& \quad b + d > 1, \tag{S.16}$$

which means that r can always be chosen so that $r_l < r < r_u$, with $r_l = \max\{a, 1-d\}$ and $r_u = \min\{b, 1-c\}$ (Fig. S.2). The object from here is to construct an asymptotic expansion for $I(\lambda)$ as either $\lambda \rightarrow 0$ or $\lambda \rightarrow \infty$. To do this consider the contour integral

$$\oint_C ds \lambda^{-s} G(s) \tag{S.17}$$

where $G(s) = M[f; 1-s] M[h; s]$ and the contour C is drawn depending on which limit of λ is chosen (Fig. S.3). If $\lambda \rightarrow 0$ (or $\lambda \rightarrow \infty$) then the contour must be closed in the left-hand (or

right-hand) plane so as to ensure that the term λ^{-s} remains finite when $\sigma \rightarrow \infty$. Treating the $\lambda \rightarrow 0$ case first, if $G(s)$ is such that $|G(\sigma \pm iN)| \rightarrow 0$ as $N \rightarrow \infty$ then the integrals along the horizontal sections will correspondingly approach zero in the same limit. Furthermore, if $G(s)$ is absolutely integrable then the integral along the vertical line at $\sigma = -R$ will be $O(\lambda^{-R})$ so that it becomes negligible as $R \rightarrow \infty$. The contour integral therefore becomes

$$\oint_C ds \lambda^{-s} G(s) = \int_{r-i\infty}^{r+i\infty} ds \lambda^{-s} G(s) = 2\pi i \sum_{\{s_n \leq r_l\}} \text{Res}\{\lambda^{-s} G(s)\} \quad (\text{S.18})$$

where $\{s_n \leq r_l\}$ is the set of all poles s_n in the left-hand plane. A similar process for the case where $\lambda \rightarrow \infty$ produces

$$\oint_C ds \lambda^{-s} G(s) = - \int_{r-i\infty}^{r+i\infty} ds \lambda^{-s} G(s) = 2\pi i \sum_{\{s_n \geq r_u\}} \text{Res}\{\lambda^{-s} G(s)\} \quad (\text{S.19})$$

with $\{s_n \geq r_u\}$ being the set of all poles in the right-hand plane. On comparison with Eq. (S.15), it is now clear that these two results provide asymptotic expansions for $I(\lambda)$ as sums over the residues at the poles of $G(s)$. That is,

$$I(\lambda) \sim \begin{cases} \sum_{\{s_n \leq r_l\}} \text{Res}\{\lambda^{-s} M[f; 1-s] M[h; s]\}, & \lambda \rightarrow 0 \\ - \sum_{\{s_n \geq r_u\}} \text{Res}\{\lambda^{-s} M[f; 1-s] M[h; s]\}, & \lambda \rightarrow \infty. \end{cases} \quad (\text{S.20})$$

Evaluation of each term in the series is aided by analytic continuation of the Mellin transform into the whole complex plane and, in particular, Eqs. (S.5) & (S.7). As noted earlier, the poles of $M[h; s]$ in the left and right halves of the complex plane correspond to the powers of x in the asymptotic expansions of $h(x)$ about 0 and ∞ , respectively. In contrast, after recalling the asymptotic expansions of $f(x)$ in Eq. (S.12), then

$$M[f; 1-s] \sim \begin{cases} - \sum_{m=0}^{M_n^0} \frac{f_{nm}^0 m!}{(s - c_n - 1)^{m+1}}, & s \rightarrow c_n + 1 \\ \sum_{m=0}^{M_n^\infty} \frac{f_{nm}^\infty m!}{(s + d_n - 1)^{m+1}}, & s \rightarrow -d_n + 1. \end{cases} \quad (\text{S.21})$$

That is, due to the shift in argument from s to $1-s$, the poles of $M[f; 1-s]$ in the left and right halves of the complex plane correspond to 1 minus the powers of x in the expansions of $f(x)$ about ∞ and 0, respectively.

S-2. Generalised methods for Mellin transforms

The Mellin transform of the function $f(x)$ was defined in Sec. S-1 under the assumption that $c < d$ so that the analytic strip is nonempty. However, when $c > d$ the integral in Eq. (S.1) does not converge so the Mellin transform in the ordinary sense does not exist. Nevertheless, analytic continuation can be used to give the Mellin transform meaning even for functions where $c > d$.

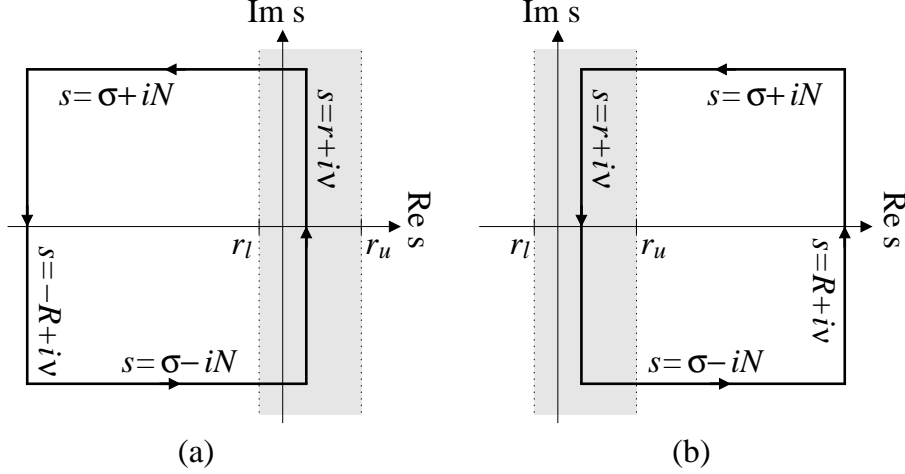


Figure S.3: Contour C used to evaluate the complex integral in Eq. (S.17) when (a) $\lambda \rightarrow 0$, and (b) $\lambda \rightarrow \infty$. Each contour consists of four lines with the parametrisation for each line written next to it. The shaded area represents the strip of analyticity $r_l < \text{Re } s < r_u$ of $G(s)$.

As in Sec. S-1, assume that $f(x)$ is locally integrable on $(0, \infty)$ and has asymptotic expansions as defined in Eq. (S.12). Now choose $x_0 > 0$ and define the functions

$$f_1(x) = \begin{cases} f(x), & 0 \leq x < x_0 \\ 0, & x_0 \leq x < \infty \end{cases} \quad (\text{S.22})$$

$$f_2(x) = f(x) - f_1(x). \quad (\text{S.23})$$

From these definitions and the contents of Sec. S-1 it is immediately true that $M[f_1; s]$ exists and has analytic strip $c < \text{Re } s$. Furthermore, $M[f_1; s]$ can be analytically continued to a meromorphic function in the left-hand plane $\text{Re } s < c$, with the asymptotic behaviour of $f_1(x)$ as $x \rightarrow 0$ dictating the behaviour of $M[f_1; s]$ at the poles. Similar characteristics hold for the analytic continuation of $M[f_2; s]$ into the right-hand plane $\text{Re } s > d$.

Now, Eq. (S.23) and the analytic continuation of $M[f_1; s]$ & $M[f_2; s]$ into the entire complex plane suggest a way to generalise the Mellin transform of $f(x)$ when $c > d$. First note that

$$M[f; s] = M[f_1; s] + M[f_2; s] \quad (\text{S.24})$$

is clearly true for the Mellin transform of $f(x)$ in the ordinary sense, i.e. when $c < d$. Moreover, the right-hand side is also well defined even when $c > d$ because both $M[f_1; s]$ and $M[f_2; s]$ exist in the ordinary sense. Using this fact, the left-hand side of Eq. (S.24) is therefore called the *Mellin transform of $f(x)$ in the generalised sense*. As all of the properties of the Mellin transform discussed in Sec. S-1 apply for $M[f_1; s]$ and $M[f_2; s]$, Eq. (S.24) also provides a means to predict the behaviour of $M[f; s]$ throughout the whole complex plane when required.

The asymptotic expansion of $I(\lambda)$ in Eq. (S.15) is now extended for the case when the Mellin transform of $f(x)$ only exists in the generalised sense. With $f_1(x)$ & $f_2(x)$ as defined in Eqs. (S.22) & (S.23) and assuming the conditions for convergence in Eq. (S.16) still apply, it is possible to write

$$I(\lambda) = \int_0^\infty dx f(x)h(\lambda x) = \int_0^\infty dx f_1(x)h(\lambda x) + \int_0^\infty dx f_2(x)h(\lambda x) = I_1(\lambda) + I_2(\lambda). \quad (\text{S.25})$$

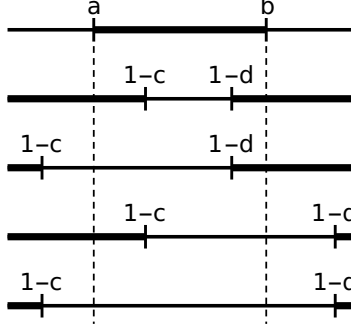


Figure S.4: Intersection between the analytic strips of $M[f; 1-s]$ and $M[h; s]$ for the case $a < b$ and $c > d$. In this case the Mellin transform of $f(x)$ only exists in the generalised sense. The upper line represents the analytic strip of $M[h; s]$, while the lower four lines represent the four distinct cases for how it may overlap the analytic strips of $M[f_1; 1-s]$ & $M[f_2; 1-s]$. Only the second line is consistent with the conditions for $I(\lambda)$ to converge (re Eq. (S.16)), in which case the intersection of the analytic strips can be summarised as $(a, 1-c) \cup (1-d, b)$. The lower three lines respectively correspond to the cases where $I_1(\lambda)$, $I_2(\lambda)$ and both $I_1(\lambda)$ & $I_2(\lambda)$ do not converge.

Setting $G_1(s) = M[h; s]M[f_1; 1-s]$, since $M[f_1; 1-s]$ and $M[h; s]$ both exist in the ordinary sense and have analytic strips that overlap for $a < \text{Re } s < 1-c$ (Fig. S.4), then the results of Sec. S-1 imply that

$$I_1(\lambda) = \frac{1}{2\pi i} \int_{r_1-i\infty}^{r_1+i\infty} ds \lambda^{-s} G_1(s) \sim \begin{cases} \sum_{\{s_n \leq a\}} \text{Res}\{\lambda^{-s} G_1(s)\}, & \lambda \rightarrow 0 \\ - \sum_{\{s_n \geq 1-c\}} \text{Res}\{\lambda^{-s} G_1(s)\}, & \lambda \rightarrow \infty, \end{cases} \quad (\text{S.26})$$

where $\{s_n \leq a\}$ & $\{s_n \geq 1-c\}$ are the pole sets in the left- and right-hand sides of the complex plane, respectively. Similarly, if $G_2(s) = M[h; s]M[f_2; 1-s]$ and realising that the analytic strips of $M[f_2; 1-s]$ and $M[h; s]$ intersect for $1-d < \text{Re } s < b$ (Fig. S.4), then

$$I_2(\lambda) = \frac{1}{2\pi i} \int_{r_2-i\infty}^{r_2+i\infty} ds \lambda^{-s} G_2(s) \sim \begin{cases} \sum_{\{s_n \leq 1-d\}} \text{Res}\{\lambda^{-s} G_2(s)\}, & \lambda \rightarrow 0 \\ - \sum_{\{s_n \geq b\}} \text{Res}\{\lambda^{-s} G_2(s)\}, & \lambda \rightarrow \infty \end{cases} \quad (\text{S.27})$$

with $\{s_n \leq 1-d\}$ & $\{s_n \geq b\}$ being the pole sets in the left- and right-hand sides of the complex plane, respectively.

Placing the series of Eqs. (S.26) & (S.27) into Eq. (S.25), the overall asymptotic expansion of $I(\lambda)$ is therefore defined to be

$$I(\lambda) \sim \begin{cases} \sum_{\{s_n \leq a\}} \text{Res}\{\lambda^{-s} G_1(s)\} + \sum_{\{s_n \leq 1-d\}} \text{Res}\{\lambda^{-s} G_2(s)\}, & \lambda \rightarrow 0 \\ - \sum_{\{s_n \geq 1-c\}} \text{Res}\{\lambda^{-s} G_1(s)\} - \sum_{\{s_n \geq b\}} \text{Res}\{\lambda^{-s} G_2(s)\}, & \lambda \rightarrow \infty. \end{cases} \quad (\text{S.28})$$

The residues in each of the series can be evaluated using Eqs. (S.5), (S.7) & (S.21) in a way that is analogous to that described in Sec. S-1.

S-3. Some details on the Mellin transforms of $h_{k0}(v)$ & $h_{kk}(v)$

It is helpful to compile a few facts about the Mellin transforms of $h_{k0}(v)$ and $h_{kk}(v)$. Starting with $h_{k0}(v)$, the singularities at $v = 0$ and ϖ_k are removable so it is a continuous and locally integrable function on $(0, \infty)$. It also has the asymptotic expansions

$$h_{k0}(v) \sim \begin{cases} \sum_{n=0}^{\infty} h_{0n}^0 v^{2n}, & v \rightarrow 0 \\ (1 - \cos v) \sum_{n=0}^{\infty} h_{0n}^{\infty} v^{-2n-4}, & v \rightarrow \infty \end{cases} \quad (\text{S.29})$$

with $h_{0n}^0 = (-)^{n+1} \sum_{m=0}^n (-)^m / [\varpi_k^{2(m+1)} (2n - 2m + 2)!]$ and $h_{0n}^{\infty} = \varpi_k^{2n}$. The powers of the leading terms in the expansions therefore stipulate that $M[h_{k0}; s]$ is analytic for the strip $0 < \text{Re } s < 4$. Moreover, from the asymptotic behaviour as $v \rightarrow 0$, $M[h_{k0}; s]$ can be analytically continued into the left-hand plane $\text{Re } s < 0$ with poles at $s = -2n$, and from the behaviour as $v \rightarrow \infty$, $M[h_{k0}; s]$ can be analytically continued into the right-hand plane $\text{Re } s > 4$ with poles at $s = 2n + 4$. Specifically,

$$M[h_{k0}; s] \sim \begin{cases} \frac{h_{0n}^0}{s + 2n}, & s \rightarrow -2n \\ -\frac{h_{0n}^{\infty}}{s - 2n - 4}, & s \rightarrow 2n + 4 \end{cases} \quad (\text{S.30})$$

for $n = 0, 1, 2, \dots$.

Next, $h_{kk}(v)$ has a removable singularity at $v = \varpi_k$ so it is also continuous and locally integrable on the positive real line. It has asymptotic expansions

$$h_{kk}(v) \sim \begin{cases} \sum_{n=0}^{\infty} h_{kn}^0 v^{2n+2}, & v \rightarrow 0 \\ (1 - \cos v) \sum_{n=0}^{\infty} h_{kn}^{\infty} v^{-2n-4}, & v \rightarrow \infty \end{cases} \quad (\text{S.31})$$

with $h_{kn}^0 = (-)^n \sum_{m=0}^n (-)^m (m + 1) / [\varpi_k^{2(m+2)} (2n - 2m + 2)!]$ and $h_{kn}^{\infty} = (n + 1) \varpi_k^{2n}$. From the leading asymptotic behaviour it can be concluded that $M[h_{kk}; s]$ is analytic in the strip $-2 < \text{Re } s < 4$. More generally, $M[h_{kk}; s]$ can be continued analytically into the whole complex plane such that

$$M[h_{kk}; s] \sim \begin{cases} \frac{h_{kn}^0}{s + 2n + 2}, & s \rightarrow -2n - 2 \\ -\frac{h_{kn}^{\infty}}{s - 2n - 4}, & s \rightarrow 2n + 4 \end{cases} \quad (\text{S.32})$$

for $n = 0, 1, 2, \dots$.

The exact values of $M[h_{k0}; s]$ and $M[h_{kk}; s]$ will also be required as coefficients in $I_{kl}^P(\beta)$ and $I_{kl}^Q(\beta)$ when s is real and not equal to a pole. In that case the Mellin transforms can be evaluated using a combination of the results presented in Sec. S-10. Using Eqs. (S.88) and (S.72), for $s \in \mathbb{R}$ it is possible to identify the correspondence

$$M[h_{k0}; s] = \lim_{s' \rightarrow s} \cos(\pi s' / 2) [H(s' - 2; 0, \varpi_k) - H(s' - 2; 1, \varpi_k)], \quad (\text{S.33})$$

where the limit is required for the case when $s = 2$ or an odd negative integer. Similarly, combining Eq. (S.88) with Eq. (S.83) enables the correspondence

$$M[h_{kk}; s] = \frac{\pi \varpi_k^{s-3}}{4} + \lim_{s' \rightarrow s} \cos(\pi s'/2) [I(s'; 0, \varpi_k) - I(s'; 1, \varpi_k)], \quad (\text{S.34})$$

with the limit again necessary for $s = 0, 2$ and odd negative integer values. Table S.1 presents exact results for selected integer and half-integer values of s .

It is useful to derive an asymptotic expansion for $M[h_{k0}; s]$ in the limit $k \rightarrow \infty$. This can be done by inserting Eqs. (S.73) & (S.74) into Eq. (S.33), and then using the identity Eq. (S.81) to write the result in terms of the incomplete Gamma function $\Gamma(z, t)$. The incomplete Gamma function has the well-known large t expansion

$$\Gamma(z, it) \sim (it)^{z-1} e^{-it} \sum_{n=0}^{\infty} \frac{\Gamma(z)}{\Gamma(z-n)} (it)^{-n},$$

which can be used to achieve the desired goal. After some manipulation to separate out the real and imaginary parts, the result is

$$M[h_{k0}; s] \sim - \lim_{s' \rightarrow s} \left\{ \frac{\pi \varpi_k^{s'-4}}{2} \cot(\pi s'/2) + \frac{\pi}{2} \csc(\pi s'/2) \sum_{n=0}^{\infty} \frac{(-)^n \varpi_k^{-2n-2}}{\Gamma(3-s'-2n)} \right\}. \quad (\text{S.35})$$

A similar procedure can be used to obtain an expansion for $M[h_{kk}; s]$. Equations (S.85) & (S.86) are placed in Eq. (S.34), and the expansion for the incomplete Gamma function is used again to derive

$$M[h_{kk}; s] \sim \frac{\pi \varpi_k^{s-3}}{4} - \lim_{s' \rightarrow s} \left\{ \frac{\pi(s'-2)\varpi_k^{s'-4}}{4} \cot(\pi s'/2) + \frac{\pi}{2} \csc(\pi s'/2) \sum_{n=0}^{\infty} \frac{(-)^n (n+1) \varpi_k^{-2n-4}}{\Gamma(1-s'-2n)} \right\}. \quad (\text{S.36})$$

S-4. Some details on the asymptotic expansion of U_{k0} & U_{kk} for Models 1 & 2

Due to the high level of repetition, only the important intermediate details of the MTM procedure have been included for Models 1 & 2. A more detailed presentation is made for Model 3 in Sec. S-5. It should also be noted that the notation is the same as that used in Sec. 2 of the main text.

Model 1.

- Spectral density:

$$u_2(\omega) = 2D_0 \left[1 - \frac{\eta}{1 + (\omega\tau)^2} \right].$$

- Expansions of $f(v)$:

$$f(v) = \frac{u_2(v/\tau)}{2D_0} = 1 - \frac{\eta}{1 + v^2} \sim \begin{cases} 1 - \eta \sum_{n=0}^{\infty} (-)^n v^{2n}, & v \rightarrow 0 \\ 1 + \eta \sum_{n=1}^{\infty} (-)^n v^{-2n}, & v \rightarrow \infty \end{cases}$$

Table S.1: Mellin transform of $h_{k0}(v)$ & $h_{kk}(v)$ for selected values of s .

| s | $M[h_{k0}; s]$ | $M[h_{kk}; s]$ |
|-------------------------------|--|---|
| $2n + 4, n = 0, 1, 2, \dots$ | <i>pole</i> | <i>pole</i> |
| $2n + 3, n = 0, 1, 2, \dots$ | 0 | $\frac{\pi \varpi_k^{2n}}{4}$ |
| 5/2 | $-\frac{\pi a_{Sk}}{2\varpi_k^{3/2}}$ | $\frac{\pi a_{Ck}}{4\varpi_k^{1/2}} - \frac{\pi a_{Sk}}{8\varpi_k^{3/2}}$ |
| 2 | $-\frac{\gamma_e + \ln \varpi_k - \text{Ci}(\varpi_k)}{\varpi_k^2}$ | $\frac{\text{Si}(\varpi_k)}{2\varpi_k}$ |
| 3/2 | $-\frac{\sqrt{2\pi}}{\varpi_k^2} + \frac{\pi a_{Ck}}{2\varpi_k^{5/2}}$ | $\frac{\sqrt{2\pi}}{4\varpi_k^2} - \frac{\pi a_{Ck}}{8\varpi_k^{5/2}} + \frac{\pi a_{Sk}}{4\varpi_k^{3/2}}$ |
| 1 | $-\frac{\pi}{2\varpi_k^2}$ | $\frac{\pi}{4\varpi_k^2}$ |
| 1/2 | $-\frac{2\sqrt{2\pi}}{3\varpi_k^2} - \frac{\pi a_{Sk}}{2\varpi_k^{7/2}}$ | $\frac{\pi a_{Ck}}{4\varpi_k^{5/2}} + \frac{3\pi a_{Sk}}{8\varpi_k^{7/2}}$ |
| 0 | <i>pole</i> | $\frac{\gamma_e + \ln \varpi_k - \text{Ci}(\varpi_k)}{\varpi_k^4} + \frac{\text{Si}(\varpi_k)}{2\varpi_k^3}$ |
| -1/2 | $-\frac{\sqrt{2\pi}}{\varpi_k^4} + \frac{4\sqrt{2\pi}}{15\varpi_k^2} + \frac{\pi a_{Ck}}{2\varpi_k^{9/2}}$ | $\frac{5\sqrt{2\pi}}{4\varpi_k^4} + \frac{\pi a_{Sk}}{4\varpi_k^{7/2}} - \frac{5\pi a_{Ck}}{8\varpi_k^{9/2}}$ |
| -1 | $\frac{\pi(\varpi_k^2 - 6)}{12\varpi_k^4}$ | $\frac{3\pi}{4\varpi_k^4}$ |
| -3 | $-\frac{\pi(\varpi_k^4 - 20\varpi_k^2 + 120)}{240\varpi_k^6}$ | $-\frac{\pi(\varpi_k^2 - 15)}{12\varpi_k^6}$ |
| -5 | $\frac{\pi(\varpi_k^6 - 42\varpi_k^4 + 840\varpi_k^2 - 5040)}{10080\varpi_k^8}$ | $\frac{\pi(\varpi_k^4 - 40\varpi_k^2 + 420)}{240\varpi_k^8}$ |
| $-2n - 2, n = 0, 1, 2, \dots$ | <i>pole</i> | <i>pole</i> |

$$\implies \theta_{1n} = \theta_{2n} = 2n, \quad f_n^0 = \delta_{n,0} - (-)^n \eta, \quad f_n^\infty = \delta_{n,0} + (1 - \delta_{n,0})(-)^n \eta.$$

- Poles of $M[f_j; 1 - s]$:

Leading terms in the expansions imply that $M[f_1; 1 - s]$ and $M[f_2; 1 - s]$ have analytic strips $\text{Re } s < 1$ and $\text{Re } s > 1$, respectively. Furthermore,

$$\begin{aligned} M[f_1; 1 - s] &\sim -\frac{f_n^0}{s - 2n - 1}, & s \rightarrow 2n + 1 \\ M[f_2; 1 - s] &\sim \frac{f_n^\infty}{s + 2n - 1}, & s \rightarrow -2n + 1 \end{aligned} \quad (n = 0, 1, 2, \dots).$$

- Pole sets of $G_{lj}(s)$:

The analytic strips of $M[f_1; 1 - s]$ and $M[h_{kl}; s]$ intersect for $-2\delta_{k,l} < \text{Re } s < 1$ so that $a_{l1} = -2\delta_{k,l}$ and $b_{l1} = 1$. Hence,

$$\begin{aligned} \{s_n \leq -2\delta_{k,l}\} &= \{-2(n + \delta_{k,l})\} = \{-2\delta_{k,l}, -2 - 2\delta_{k,l}, -4 - 2\delta_{k,l}, \dots\} \\ \{s_n \geq 1\} &= \{2(n + 2)\} \cup \{2n + 1\} = \{4, 6, 8, \dots\} \cup \{1, 3, 5, \dots\} \\ \implies Q_{l1} &= \emptyset, \quad P_{l1} = R_{l1} = \{0, 1, 2, \dots\}. \end{aligned}$$

The analytic strips of $M[f_2; 1 - s]$ and $M[h_{kl}; s]$ intersect for $1 < \text{Re } s < 4$ so that $a_{l2} = 1$ and $b_{l2} = 4$. It follows that

$$\begin{aligned} \{s_n \leq 1\} &= \{-2(n + \delta_{k,l})\} \cup \{-2n + 1\} \\ &= \{-2\delta_{k,l}, -2 - 2\delta_{k,l}, -4 - 2\delta_{k,l}, \dots\} \cup \{1, -1, -3, -5, \dots\} \\ \{s_n \geq 4\} &= \{2(n + 2)\} = \{4, 6, 8, \dots\} \\ \implies Q_{l2} &= \emptyset, \quad P_{l2} = R_{l2} = \{0, 1, 2, \dots\}. \end{aligned}$$

- Exact Mellin transform of $f(v)$:

Using Eqs. (S.72), (S.73) & (S.87),

$$M[f; s] = M[1; s] - \eta H(s; 0, 1) = -\frac{\pi\eta}{2 \sin(\pi s/2)}.$$

- Combining the results:

$$I_{kl}^P(\beta) \sim \begin{cases} M[h_{kl}; 1] \beta^{-1} - \eta M[h_{kl}; -1] \beta + \eta M[h_{kl}; -3] \beta^3 + O(\beta^5), & \beta \rightarrow 0 \\ (1 - \eta) M[h_{kl}; 1] \beta^{-1} + \eta M[h_{kl}; 3] \beta^{-3} - \eta M[h_{kl}; 5] \beta^{-5} + O(\beta^{-7}), & \beta \rightarrow \infty \end{cases}$$

$$I_{kl}^R(\beta) \sim \begin{cases} -\frac{\pi\eta}{4\varpi_k^{2+2\delta_{k,l}}} \beta^{2\delta_{k,l}} + \frac{\pi\eta[\varpi_k^2 - 12(1 + \delta_{k,l})]}{48\varpi_k^{4+2\delta_{k,l}}} \beta^{2+2\delta_{k,l}} + O(\beta^{4+2\delta_{k,l}}), & \beta \rightarrow 0 \\ -\frac{\pi\eta}{2} \beta^{-4} + O(\beta^{-6}), & \beta \rightarrow \infty \end{cases}$$

Model 2.

- Spectral density:

$$u_2(\omega) = 2D_0 \left[1 - \zeta \frac{1 - \sqrt{|\omega|\tau/2} + |\omega|\tau\sqrt{|\omega|\tau/2}}{1 + (\omega\tau)^2} \right]$$

- Expansions of $f(v)$:

$$f(v) = \frac{u_2(v/\tau)}{2D_0} = 1 - \zeta \frac{1 - \sqrt{v/2} + v\sqrt{v/2}}{1 + v^2}$$

$$\sim \begin{cases} 1 - \zeta \left(1 - \frac{v^{1/2}}{\sqrt{2}} + \frac{v^{3/2}}{\sqrt{2}} \right) \sum_{n=0}^{\infty} (-)^n v^{2n}, & v \rightarrow 0 \\ 1 + \zeta \left(1 - \frac{v^{1/2}}{\sqrt{2}} + \frac{v^{3/2}}{\sqrt{2}} \right) \sum_{n=1}^{\infty} (-)^n v^{-2n}, & v \rightarrow \infty \end{cases}$$

$$\implies \theta_{1n} = \theta_{2n} = \varphi_n/2, \quad f_n^0 = \delta_{n,0} - \zeta \operatorname{Re} \alpha_2 \varphi_n \quad f_n^\infty = \delta_{n,0} + (1 - \delta_{n,0}) \zeta \operatorname{Re} (-\alpha_1) \varphi_n$$

where $\varphi_n = n + \lfloor (n+1)/3 \rfloor$, $\alpha_1 = \sqrt{i}$ and $\alpha_2 = i\sqrt{i}$.

- Poles of $M[f_j; 1-s]$:

$M[f_1; 1-s]$ and $M[f_2; 1-s]$ have analytic strips $\operatorname{Re} s < 1$ and $\operatorname{Re} s > 1$, respectively. Also,

$$M[f_1; 1-s] \sim -\frac{f_n^0}{s - \varphi_n/2 - 1}, \quad s \rightarrow \varphi_n/2 + 1$$

$$M[f_2; 1-s] \sim \frac{f_n^\infty}{s + \varphi_n/2 - 1}, \quad s \rightarrow -\varphi_n/2 + 1$$

($n = 0, 1, 2, \dots$).

- Pole sets of $G_{lj}(s)$:

The analytic strips of $M[f_1; 1-s]$ and $M[h_{kl}; s]$ intersect for $-2\delta_{k,l} < \operatorname{Re} s < 1$ so that $a_{l1} = -2\delta_{k,l}$ and $b_{l1} = 1$. Hence,

$$\{s_n \leq -2\delta_{k,l}\} = \{-2(n + \delta_{k,l})\} = \{-2\delta_{k,l}, -2 - 2\delta_{k,l}, -4 - 2\delta_{k,l}, \dots\}$$

$$\{s_n \geq 1\} = \{2(n+2)\} \cup \{\varphi_n/2 + 1\} = \{4, 6, 8, \dots\} \cup \{1, 3/2, 5/2, 3, 7/2, \dots\}$$

$$\implies Q_{l1} = \emptyset, \quad P_{l1} = R_{l1} = \{0, 1, 2, \dots\}.$$

The analytic strips of $M[f_2; 1-s]$ and $M[h_{kl}; s]$ intersect for $1 < \operatorname{Re} s < 4$ so that $a_{l2} = 1$ and $b_{l2} = 4$. It follows that

$$\{s_n \leq 1\} = \{-2(n + \delta_{k,l})\} \cup \{-\varphi_n/2 + 1\}$$

$$= \{-2\delta_{k,l}, -2 - 2\delta_{k,l}, -4 - 2\delta_{k,l}, \dots\} \cup \{1, 1/2, -1/2, -1, \dots\}$$

$$\{s_n \geq 4\} = \{2(n+2)\} = \{4, 6, 8, \dots\}$$

$$\implies Q_{l2} = \emptyset, \quad P_{l2} = R_{l2} = \{0, 1, 2, \dots\}.$$

- Exact Mellin transform of $f(v)$:

From Eqs. (S.72), (S.73) & (S.87),

$$M[f; s] = M[1; s] - \zeta \left[H(s; 0, 1) - \frac{H(s + 1/2; 0, 1)}{\sqrt{2}} + \frac{H(s + 3/2; 0, 1)}{\sqrt{2}} \right] = -\frac{2\pi\zeta \cos(\pi s/2)}{\sin(2\pi s)}.$$

- Keeping only a few of the most dominant terms:

$$I_{kl}^P(\beta) \sim \begin{cases} M[h_{kl}; 1] \beta^{-1} - \frac{\zeta}{\sqrt{2}} M[h_{kl}; 1/2] \beta^{-1/2} \\ \quad + \frac{\zeta}{\sqrt{2}} M[h_{kl}; -1/2] \beta^{1/2} + O(\beta), & \beta \rightarrow 0 \\ (1 - \zeta) M[h_{kl}; 1] \beta^{-1} + \frac{\zeta}{\sqrt{2}} M[h_{kl}; 3/2] \beta^{-3/2} \\ \quad - \frac{\zeta}{\sqrt{2}} M[h_{kl}; 5/2] \beta^{-5/2} + O(\beta^{-3}), & \beta \rightarrow \infty \end{cases}$$

$$I_{kl}^R(\beta) \sim \begin{cases} -\frac{\pi\zeta}{4\varpi_k^{2+2\delta_{k,l}}} \beta^{2\delta_{k,l}} - \frac{\pi\zeta[\varpi_k^2 - 12(1 + \delta_{k,l})]}{48\varpi_k^{4+2\delta_{k,l}}} \beta^{2+2\delta_{k,l}} + O(\beta^{4+2\delta_{k,l}}), & \beta \rightarrow 0 \\ \frac{\pi\zeta}{2} \beta^{-4} + O(\beta^{-6}), & \beta \rightarrow \infty \end{cases}$$

S-5. Asymptotic expansion of U_{k0} & U_{kk} for Model 3

The dispersive diffusivity of this model is

$$\mathcal{D}(\omega) = \frac{D_0}{1 + \zeta + 2z_\omega \left[\sqrt{\zeta + (1 - z_\omega)^2} - (1 - z_\omega) \right]},$$

where $z_\omega = i\sqrt{i\omega\tau}$. Although a closed form for $u_2(\omega) = 2\text{Re } \mathcal{D}(\omega)$ can be obtained, the derivation is tedious and contains awkward nested square roots. A simpler way to obtain the asymptotic behaviour of $u_2(\omega)$ is to use the expansions for $\mathcal{D}(\omega)$

$$\frac{\mathcal{D}(\omega)}{D_0} \sim \begin{cases} \sum_{n=0}^{\infty} d_n^0 \alpha_2^n (\omega\tau)^{n/2}, & \omega\tau \rightarrow 0 \\ \sum_{n=0}^{\infty} (-)^n d_n^\infty \alpha_1^n (\omega\tau)^{-n/2}, & \omega\tau \rightarrow \infty \end{cases} \quad (\text{S.37})$$

with

$$\begin{aligned} d_0^0 &= 1/(1 + \zeta) & d_0^\infty &= 1 \\ d_1^0 &= 2[1 - \sqrt{1 + \zeta}]/(1 + \zeta)^2 & d_1^\infty &= \zeta \\ d_2^0 &= 2[3 + \zeta - 3\sqrt{1 + \zeta}]/(1 + \zeta)^3, & d_2^\infty &= \zeta[4 + 3\zeta]/4 \end{aligned}$$

Table S.2: α_1 and α_2 generate the cyclic group of order 8.

| n | 0 | 1 | 2 | 3 | 4 | 5 | 6 | 7 | 8 |
|--------------|---|-------------|------|------------|----|-------------|------|-------------|---|
| α_1^n | 1 | \sqrt{i} | i | α_2 | -1 | $-\alpha_1$ | $-i$ | $-\alpha_2$ | 1 |
| α_2^n | 1 | $i\sqrt{i}$ | $-i$ | α_1 | -1 | $-\alpha_2$ | i | $-\alpha_1$ | 1 |

$$\begin{aligned}
 d_3^0 &= [16 + 8\zeta - (16 + \zeta)\sqrt{1 + \zeta}]/(1 + \zeta)^4 & d_3^\infty &= \zeta[4 + 5\zeta + 2\zeta^2]/4 \\
 d_4^0 &= [40 + 24\zeta - (40 + 5\zeta)\sqrt{1 + \zeta}]/(1 + \zeta)^5 & d_4^\infty &= \zeta[16 + 24\zeta + 18\zeta^2 + 5\zeta^3]/16
 \end{aligned}$$

being the first five coefficients in both expansions. The coefficients d_n^0 and d_n^∞ are all real numbers so that the complex nature of the function is completely retained in the numbers $\alpha_1 = \sqrt{i} = (1+i)/\sqrt{2}$ and $\alpha_2 = i\sqrt{i} = (-1+i)/\sqrt{2}$, which are both 8th complex roots of unity and hence generate the cyclic group of order 8 under multiplication (see Table S.2). This means that expansions for $u_2(\omega)$ can be constructed by simply omitting the terms in Eq. (S.37) with $n = 4l + 2$ ($l = 0, 1, 2, \dots$) because $\text{Re } \alpha_1^n = \text{Re } \alpha_2^n = 0$ for those values of n . Explicitly,

$$\frac{u_2(\omega)}{2D_0} \sim \begin{cases} d_0^0 - \frac{d_1^0}{\sqrt{2}}(\omega\tau)^{\frac{1}{2}} + \frac{d_3^0}{\sqrt{2}}(\omega\tau)^{\frac{3}{2}} - d_4^0(\omega\tau)^2 + O(\omega\tau)^{\frac{5}{2}}, & \omega\tau \rightarrow 0 \\ d_0^\infty - \frac{d_1^\infty}{\sqrt{2}}(\omega\tau)^{-\frac{1}{2}} + \frac{d_3^\infty}{\sqrt{2}}(\omega\tau)^{-\frac{3}{2}} - d_4^\infty(\omega\tau)^{-2} + O(\omega\tau)^{-\frac{5}{2}}, & \omega\tau \rightarrow \infty. \end{cases} \quad (\text{S.38})$$

Now to consider $f(v) = u(v/\tau)/2D_0$, the expansions in the previous paragraph imply that

$$f(v) \sim \begin{cases} \sum_{n=0}^{\infty} f_n^0 v^{\varphi_n/2}, & v \rightarrow 0 \\ \sum_{n=0}^{\infty} f_n^\infty v^{-\varphi_n/2}, & v \rightarrow \infty \end{cases} \quad (\text{S.39})$$

where $\varphi_n = n + \lfloor (n+1)/3 \rfloor$, $f_n^0 = d_{\varphi_n}^0 \text{Re } \alpha_2^{\varphi_n}$ and $f_n^\infty = d_{\varphi_n}^\infty \text{Re } (-\alpha_1)^{\varphi_n}$. It is evident from the powers of the leading terms that the analytic strip of $M[f; s]$ is empty, which means that the generalised methods of Sec. S-2 must be used to evaluate the Mellin transform of $f(v)$. Choose $v_0 \in (0, \infty)$ and then define $f_1(v) = f(v)$ for $0 \leq v < v_0$, $f_1(v) = 0$ for $v_0 \leq v$ and $f_2(v) = f(v) - f_1(v)$. From the behaviour of $f_1(v)$ as $v \rightarrow 0$, $M[f_1; s]$ is analytic for $\text{Re } s > 0$ and can be analytically continued to $\text{Re } s < 0$ with $M[f_1; s] \sim f_n^0/(s + \varphi_n/2)$ as $s \rightarrow -\varphi_n/2$. Similarly, from the behaviour of $f_2(v)$ as $v \rightarrow \infty$, $M[f_2; s]$ is analytic for $\text{Re } s < 0$ and can be analytically continued to $\text{Re } s > 0$ with $M[f_2; s] \sim -f_n^\infty/(s - \varphi_n/2)$ as $s \rightarrow \varphi_n/2$. After shifting s to $1 - s$ it is clear that $M[f_1; 1 - s]$ and $M[f_2; 1 - s]$ have analytic strips $\text{Re } s < 1$ and $\text{Re } s > 1$, respectively, and that

$$M[f_1; 1 - s] \sim -\frac{f_n^0}{s - \varphi_n/2 - 1}, \quad s \rightarrow \varphi_n/2 + 1 \quad (\text{S.40})$$

$$M[f_2; 1 - s] \sim \frac{f_n^\infty}{s + \varphi_n/2 - 1}, \quad s \rightarrow -\varphi_n/2 + 1. \quad (\text{S.41})$$

The Mellin transform technique will be applied for U_{k0} first. It is clear from Sec. S-4 and the results above that the analytic strips of $M[f_1; 1 - s]$ and $M[h_{k0}; s]$ intersect for $0 < \text{Re } s < 1$, and

the analytic strips of $M[f_2; 1 - s]$ and $M[h_{k0}; s]$ intersect for $1 < \text{Re } s < 4$. With reference to Eqs. (S.15) & (S.25), this means that it is valid to write

$$\begin{aligned} I_{k0}(\beta) &= \int_0^\infty dv [f_1(v) + f_2(v)] h_{k0}(\beta v) \\ &= \frac{1}{2\pi i} \int_{c_1 - i\infty}^{c_1 + i\infty} ds \beta^{-s} G_{01}(s) + \frac{1}{2\pi i} \int_{c_2 - i\infty}^{c_2 + i\infty} ds \beta^{-s} G_{02}(s) \end{aligned}$$

for $c_1 \in (0, 1)$, $c_2 \in (1, 4)$ and $G_{0j}(s) = M[f_j; 1 - s]M[h_{k0}; s]$, $j = 1, 2$. The analog of Eq. (S.28) therefore applies

$$I_{k0}(\beta) \sim \begin{cases} \sum_{\{s_n \leq 0\}} \text{Res}\{\beta^{-s} G_{01}(s)\} + \sum_{\{s_n \leq 1\}} \text{Res}\{\beta^{-s} G_{02}(s)\}, & \beta \rightarrow 0 \\ -\sum_{\{s_n \geq 1\}} \text{Res}\{\beta^{-s} G_{01}(s)\} - \sum_{\{s_n \geq 4\}} \text{Res}\{\beta^{-s} G_{02}(s)\}, & \beta \rightarrow \infty \end{cases} \quad (\text{S.42})$$

with $n = 0, 1, 2, \dots$. The set of poles of $G_{01}(s)$ is a union of the poles of $M[f_1; 1 - s]$ and $M[h_{k0}; s]$:

$$\begin{aligned} \text{left-hand plane:} & \quad \{s_n \leq 0\} = \{-2n\} = \{0, -2, -4, \dots\} \\ \text{right-hand plane:} & \quad \{s_n \geq 1\} = \{2n + 4\} \cup \{\varphi_n/2 + 1\} = \{1, 3/2, 5/2, \dots\}, \end{aligned}$$

and the set of poles of $G_{02}(s)$ is a union of the poles of $M[f_2; 1 - s]$ and $M[h_{k0}; s]$:

$$\begin{aligned} \text{left-hand plane:} & \quad \{s_n \leq 1\} = \{-2n\} \cup \{-\varphi_n/2 + 1\} = \{1, 1/2, 0, -1/2, \dots\} \\ \text{right-hand plane:} & \quad \{s_n \geq 4\} = \{2n + 4\} = \{4, 6, \dots\}. \end{aligned}$$

The poles have been ordered on the far right according to the significance of the corresponding power of β as it approaches 0 or ∞ . As there are no repetitions in any of the sets, it follows that

$$Q_{01} = Q_{02} = \emptyset, \quad P_{01} = R_{01} = P_{02} = R_{02} = \{0, 1, 2, \dots\}.$$

The poles are all simple so it is relatively easy to calculate the residues to obtain

$$I_{k0}^P(\beta) \sim \begin{cases} \sum_{n=0}^{\infty} \beta^{\varphi_n/2-1} f_n^\infty M[h_{k0}; -\varphi_n/2 + 1], & \beta \rightarrow 0 \\ \sum_{n=0}^{\infty} \beta^{-\varphi_n/2-1} f_n^0 M[h_{k0}; \varphi_n/2 + 1], & \beta \rightarrow \infty \end{cases} \quad (\text{S.43})$$

$$I_{k0}^R(\beta) \sim \begin{cases} \sum_{n=0}^{\infty} \beta^{2n} h_{0n}^0 M[f; 2n + 1], & \beta \rightarrow 0 \\ \sum_{n=0}^{\infty} \beta^{-2n-4} h_{0n}^\infty M[f; -2n - 3], & \beta \rightarrow \infty \end{cases} \quad (\text{S.44})$$

where $M[f; 2n + 1]$ and $M[f; -2n - 3]$ are used in the generalised sense of Eq. (S.24).

Following a similar process for U_{kk} now, the strips of analyticity of $M[f_1; 1-s]$ and $M[h_{kk}; s]$ intersect for $-2 < \text{Re } s < 1$, and those for $M[f_2; 1-s]$ and $M[h_{kk}; s]$ intersect for $1 < \text{Re } s < 4$. Using Eqs. (S.15) & (S.25) again

$$\begin{aligned} I_{kk}(\beta) &= \int_0^\infty dv [f_1(v) + f_2(v)] h_{kk}(\beta v) \\ &= \frac{1}{2\pi i} \int_{c_1-i\infty}^{c_1+i\infty} ds \beta^{-s} G_{k1}(s) + \frac{1}{2\pi i} \int_{c_2-i\infty}^{c_2+i\infty} ds \beta^{-s} G_{k2}(s) \end{aligned}$$

with $c_1 \in (-2, 1)$, $c_2 \in (1, 4)$ and $G_{kj}(s) = M[f_j; 1-s]M[h_{kk}; s]$, $j = 1, 2$. Subsequently, Eq. (S.28) implies that

$$I_{kk}(\beta) \sim \begin{cases} \sum_{\{s_n \leq -2\}} \text{Res}\{\beta^{-s} G_{k1}(s)\} + \sum_{\{s_n \leq 1\}} \text{Res}\{\beta^{-s} G_{k2}(s)\}, & \beta \rightarrow 0 \\ -\sum_{\{s_n \geq 1\}} \text{Res}\{\beta^{-s} G_{k1}(s)\} - \sum_{\{s_n \geq 4\}} \text{Res}\{\beta^{-s} G_{k2}(s)\}, & \beta \rightarrow \infty \end{cases} \quad (\text{S.45})$$

for $n = 0, 1, 2, \dots$. Combining the poles of $M[f_1; 1-s]$ and $M[h_{kk}; s]$ to obtain the poles of $G_{k1}(s)$:

$$\begin{aligned} \text{left-hand plane:} & \quad \{s_n \leq -2\} = \{-2n - 2\} = \{-2, -4, \dots\} \\ \text{right-hand plane:} & \quad \{s_n \geq 1\} = \{2n + 4\} \cup \{\varphi_n/2 + 1\} = \{1, 3/2, 5/2, \dots\}, \end{aligned}$$

and similarly merging the poles of $M[f_2; 1-s]$ and $M[h_{kk}; s]$ as the set of poles of $G_{k2}(s)$:

$$\begin{aligned} \text{left-hand plane:} & \quad \{s_n \leq 1\} = \{-2n - 2\} \cup \{-\varphi_n/2 + 1\} = \{1, 1/2, -1/2, \dots\} \\ \text{right-hand plane:} & \quad \{s_n \geq 4\} = \{2n + 4\} = \{4, 6, \dots\}. \end{aligned}$$

The poles are all simple with no repetitions so

$$Q_{01} = Q_{02} = \emptyset, \quad P_{01} = R_{01} = P_{02} = R_{02} = \{0, 1, 2, \dots\}.$$

After calculating the residues

$$I_{kk}^P(\beta) \sim \begin{cases} \sum_{n=0}^{\infty} \beta^{\varphi_n/2-1} f_n^\infty M[h_{kk}; -\varphi_n/2 + 1], & \beta \rightarrow 0 \\ \sum_{n=0}^{\infty} \beta^{-\varphi_n/2-1} f_n^0 M[h_{kk}; \varphi_n/2 + 1], & \beta \rightarrow \infty \end{cases} \quad (\text{S.46})$$

$$I_{kk}^R(\beta) \sim \begin{cases} \sum_{n=0}^{\infty} \beta^{2n+2} h_{kn}^0 M[f; 2n + 3], & \beta \rightarrow 0 \\ \sum_{n=0}^{\infty} \beta^{-2n-4} h_{kn}^\infty M[f; -2n - 3], & \beta \rightarrow \infty \end{cases} \quad (\text{S.47})$$

with $M[f; 2n + 3]$ and $M[f; -2n - 3]$ used to represent the generalised Mellin transform in the sense of Eq. (S.24).

The Mellin transforms of $h_{k0}(v)$ and $h_{kk}(v)$ that appear as coefficients in Eqs. (S.43) & (S.46) can be inserted from Table S.1. Unfortunately, a closed form for the coefficients involving the Mellin transform of $f(v)$ is not available. However, as it is only the value that is required rather than the functional form of the result, given specific s and ζ those coefficients can be obtained with numerical techniques. The method outlined on page 117 of [9] must be used to do this because the analytic strip of $M[f; 1-s]$ is empty.

Inserting the information from Eqs. (S.43), (S.44), (S.46) & (S.47) into Eq. (6), and recalling that $\beta = \varpi_k/\omega_k\tau$, the final results are

$$\frac{U_{k0}}{2D_0} \sim \begin{cases} d_0^0 - A_{01}^\infty \frac{d_1^0}{\sqrt{2}} (\omega_k\tau)^{\frac{1}{2}} + A_{03}^\infty \frac{d_3^0}{\sqrt{2}} (\omega_k\tau)^{\frac{3}{2}} + O(\omega_k\tau)^2, & \omega_k\tau \rightarrow 0 \\ d_0^\infty - A_{01}^0 \frac{d_1^\infty}{\sqrt{2}} (\omega_k\tau)^{-\frac{1}{2}} + kM[f; 1](\omega_k\tau)^{-1} + O(\omega_k\tau)^{-\frac{3}{2}}, & \omega_k\tau \rightarrow \infty \end{cases} \quad (\text{S.48})$$

$$A_{01}^\infty = \frac{2}{\pi k^{1/2}} - \frac{a_{Ck}}{\varpi_k}, \quad A_{03}^\infty = \frac{a_{Sk}}{\varpi_k}, \quad A_{01}^0 = \frac{8k^{1/2}}{3} + \frac{a_{Sk}}{\varpi_k}.$$

$$\frac{U_{kk}}{2D_0} \sim \begin{cases} d_0^0 - A_{k1}^\infty \frac{d_1^0}{\sqrt{2}} (\omega_k\tau)^{\frac{1}{2}} + A_{k3}^\infty \frac{d_3^0}{\sqrt{2}} (\omega_k\tau)^{\frac{3}{2}} + O(\omega_k\tau)^2, & \omega_k\tau \rightarrow 0 \\ d_0^\infty - A_{k1}^0 \frac{d_1^\infty}{\sqrt{2}} (\omega_k\tau)^{-\frac{1}{2}} + A_{k3}^0 \frac{d_3^\infty}{\sqrt{2}} (\omega_k\tau)^{-\frac{3}{2}} + O(\omega_k\tau)^{-2}, & \omega_k\tau \rightarrow \infty \end{cases} \quad (\text{S.49})$$

$$\begin{aligned} A_{k1}^\infty &= \frac{1}{\pi k^{1/2}} - \frac{a_{Ck}}{2\varpi_k} + a_{Sk} & A_{k3}^\infty &= -\frac{a_{Sk}}{2\varpi_k} + a_{Ck} \\ A_{k1}^0 &= \frac{3a_{Sk}}{2\varpi_k} + a_{Ck} & A_{k3}^0 &= \frac{5}{\pi k^{1/2}} - \frac{5a_{Ck}}{2\varpi_k} + a_{Sk}. \end{aligned}$$

Here $a_{Sk} = 2S(2k^{1/2})$ and $a_{Ck} = 2C(2k^{1/2})$ where $S(z)$ and $C(z)$ are the Fresnel integrals. The coefficients A_{0n}^∞ , A_{0n}^0 , A_{kn}^∞ and A_{kn}^0 have been used to help identify differences in the asymptotic behaviour of U_{k0} & U_{kk} in comparison to that of $u_2(\omega_k)$ (re Eq. (S.38)).

S-6. Structural universality

The goal here is to derive the asymptotic behaviour of U_{k0} and U_{kk} given only the information in Eq. (5). It shall simply be assumed that all of the conditions hold for the MTM to be applied. It shall also be assumed that there is a time-scale with respect to which the asymptotic frequency-dependence of the model may be investigated. As there is no obvious choice for such a time-scale in the given information, an unspecified parameter τ shall be introduced in the following so that the problem can be written in the dimensionless form of Eq. (6).

The first step in the procedure is to note that, after making the variable change $v = \omega\tau$ in Eq. (5),

$$2D_0 f(v) = u_2(v/\tau) \sim \begin{cases} 2D_\infty + (c_\infty/\tau^\vartheta) v^\vartheta, & v \rightarrow 0 \\ 2D_0 - (c_0\tau^{1/2}) v^{-1/2}, & v \rightarrow \infty. \end{cases} \quad (\text{S.50})$$

With respect to the notation in Eq. (12) it follows that

$$\{\theta_{1n}\} = \{0, \vartheta, \dots\}, \quad \{f_n^0\} = \{D_\infty/D_0, c_\infty/2\tau^\vartheta D_0, \dots\} \quad (\text{S.51})$$

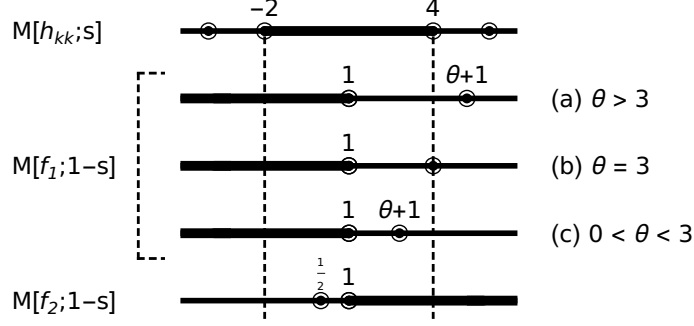


Figure S.5: Illustration demonstrating how the analytic strips and known poles of $M[f_1; 1-s]$ & $M[f_2; 1-s]$ are positioned along the real axis of the complex plane relative to the analytic strip and poles of $M[h_{kk}; s]$. There are 3 separate cases depending on the value of ϑ .

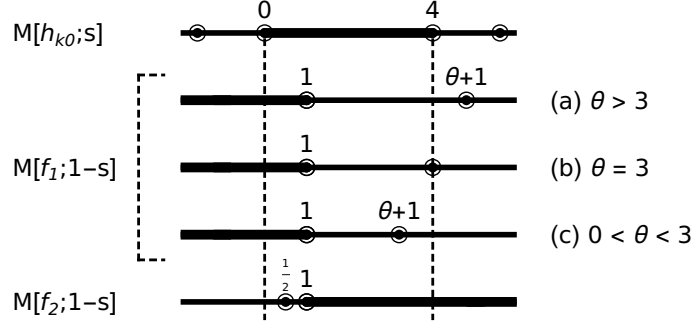


Figure S.6: Illustration demonstrating how the analytic strips and known poles of $M[f_1; 1-s]$ & $M[f_2; 1-s]$ are positioned along the real axis of the complex plane relative to the analytic strip and poles of $M[h_{k0}; s]$. There are 3 separate cases depending on the value of ϑ .

$$\{\theta_{2n}\} = \{0, 1/2, \dots\}, \quad \{f_n^\infty\} = \{1, -c_0\tau^{1/2}/2D_0, \dots\}. \quad (\text{S.52})$$

The values of θ_{10} & θ_{20} imply that the analytic strip of $M[f; s]$ is empty so the generalised Mellin transform must be used. Defining $f_1(v)$ & $f_2(v)$ as in Eqs. (7) & (8), it can be said that $M[f_1; 1-s]$ is analytic for $\text{Re } s < 1$ while $M[f_2; 1-s]$ is analytic for $\text{Re } s > 1$. Furthermore, analytic continuation into the entire complex plane implies that

$$M[f_1; 1-s] \sim \begin{cases} -\frac{f_0^0}{s-1}, & s \rightarrow 1 \\ -\frac{f_1^0}{s-\vartheta-1}, & s \rightarrow \vartheta+1 \end{cases} \quad (\text{S.53})$$

$$M[f_2; 1-s] \sim \begin{cases} \frac{f_0^\infty}{s-1}, & s \rightarrow 1 \\ \frac{f_1^\infty}{s-1/2}, & s \rightarrow 1/2. \end{cases} \quad (\text{S.54})$$

If required the Mellin transform of $f(v)$ can be evaluated using $M[f; 1-s] = M[f_1; 1-s] + M[f_2; 1-s]$. Note that, due to the limited number of terms in the asymptotic expansions given for $u_2(\omega)$, nothing is known about the behaviour of $M[f; 1-s]$ beyond the poles at $\vartheta+1$, $1/2$ and 1 .

The next step is to consider how the exponent ϑ affects the problem. With reference to the conditions in Eq. (S.16), $I_{kl}(\beta)$ is convergent for $\vartheta > -1 - 2\delta_{k,l}$, which is always satisfied because $\vartheta > 0$. Therefore, the value of ϑ only affects the problem through the positions of the known poles of $M[f_1; 1-s]$ relative to the poles of $M[h_{kl}; s]$ (Figs. S.5 & S.6). There are three separate cases:

- (a) $0 < \vartheta < 3$. The analytic strip of $M[f_1; 1-s]$ intersects with that of $M[h_{kl}; s]$ for $-2\delta_{k,l} < \text{Re } s < 1$, which means that the known poles of $G_{l1}(s)$ are

$$\begin{aligned} \text{left-hand plane:} & \quad \{s_n \leq -2\delta_{k,l}\} = \{-2n - 2\delta_{k,l}\} = \{-2\delta_{k,l}, -2 - 2\delta_{k,l}, \dots\} \\ \text{right-hand plane:} & \quad \{s_n \geq 1\} = \{2n + 4\} \cup \{1, \vartheta + 1\} = \{1, \vartheta + 1, 4, \dots\}. \end{aligned}$$

Similarly, the analytic regions of $M[f_2; 1-s]$ and $M[h_{kl}; s]$ overlap for $1 < \text{Re } s < 4$ so the known poles of $G_{l2}(s)$ are

$$\begin{aligned} \text{left-hand plane:} & \quad \{s_n \leq 1\} = \{-2n - 2\delta_{k,l}\} \cup \{1, 1/2\} = \{1, 1/2, \dots, -2\delta_{k,l}, \dots\} \\ \text{right-hand plane:} & \quad \{s_n \geq 4\} = \{2n + 4\} = \{4, \dots\}. \end{aligned}$$

There are no repetitions so

$$Q_{l1} = Q_{l2} = \emptyset, \quad P_{l1} = P_{l2} = \{0, 1\}, \quad R_{l1} = R_{l2} = \{0, 1, 2, \dots\}. \quad (\text{S.55})$$

The residues are easy to calculate because the poles are simple, and so

$$I_{kl}^P(\beta) \sim \begin{cases} f_0^\infty M[h_{kl}; 1]\beta^{-1} + f_1^\infty M[h_{kl}; 1/2]\beta^{-1/2}, & \beta \rightarrow 0 \\ f_0^0 M[h_{kl}; 1]\beta^{-1} + f_1^0 M[h_{kl}; \vartheta + 1]\beta^{-\vartheta-1}, & \beta \rightarrow \infty \end{cases} \quad (\text{S.56})$$

$$I_{kl}^R(\beta) \sim \begin{cases} h_{l0}^0 M[f; 1 + 2\delta_{k,l}]\beta^{2\delta_{k,l}}, & \beta \rightarrow 0 \\ h_{l0}^\infty M[f; -3]\beta^{-4}, & \beta \rightarrow \infty \end{cases} \quad (\text{S.57})$$

- (b) $\vartheta = 3$. Even though the intersection of the analytic regions of $M[f_1; 1-s]$ and $M[h_{kl}; s]$ is the same as for case (a), in this special case the pole $\vartheta + 1 = 4$ of $M[f_1; 1-s]$ coincides with the first pole of $M[h_{kl}; s]$ so that $G_{l1}(s)$ has a second order pole. Accordingly,

$$\{s_n \geq 1\} = \{2n + 4\} \cup \{1, \vartheta + 1\} = \{1, (4, 4), \dots\}$$

and $Q_{l1} = \{(1, 0)\}$, $P_{l1} = \{0\}$ & $R_{l1} = \{1, 2, 3, \dots\}$. It follows that for $\beta \rightarrow \infty$,

$$\begin{aligned} I_{kl}^P(\beta) & \sim f_0^0 M[h_{kl}; 1]\beta^{-1} \\ I_{kl}^R(\beta) & \sim O(\beta^{-6}) \\ I_{kl}^Q(\beta) & \sim h_{l0}^\infty f_1^0 \beta^{-4} \ln \beta + K_{l10}^1 \beta^{-4} \end{aligned}$$

with

$$K_{l10}^1 = h_{l0}^\infty M[f_2; -3] - \lim_{s \rightarrow 4} \frac{d}{ds} \{(s-4)^2 G_{l1}(s)\}.$$

As ϑ does not affect the expansion as $\beta \rightarrow 0$, from here on the details for that limit are the same as for case (a) above.

(c) $\vartheta > 3$. The only difference between this case and case (a) is the order of the poles of $G_{l1}(s)$ in the right-hand plane. That is,

$$\{s_n \geq 1\} = \{2n + 4\} \cup \{1, \vartheta + 1\} = \{1, 4, \vartheta + 1, \dots\}.$$

Otherwise, the sets Q_{l1} , P_{l1} & R_{l1} are unaltered from those in Eq. (S.55) so $I_{kl}^P(\beta)$ & $I_{kl}^R(\beta)$ are the same as in Eqs. (S.56) & (S.57), respectively. It must be remembered though that, as $\beta \rightarrow \infty$, the leading $O(\beta^{-4})$ term in $I_{kl}^R(\beta)$ now dominates the $O(\beta^{-\vartheta-1})$ term in $I_{kl}^P(\beta)$ when the two quantities are summed to form $I_{kl}(\beta)$.

Recalling Eq. (6) and the fact that $\beta = \varpi_k/\omega_k\tau$ and $f(v) = u_2(v/\tau)/2D_0$, the preceding information enables the known terms in the expansions of U_{kk} to be summarised. For the high-frequency limit,

$$U_{kk} \sim 2D_0 - C_{k1}^0 \omega_k^{-1/2} + \dots + C_{k2}^0 \omega_k^{-3}, \quad \omega_k\tau \rightarrow \infty$$

where

$$C_{k1}^0/c_0 = a_{ck} + 3a_{sk}/2\varpi_k = A_{k1}^0 \quad C_{k2}^0 = 4\varpi_k D_0 M[f; 3]/\pi\tau^3.$$

For the low-frequency limit, $\omega_k\tau \rightarrow 0$, the qualitative behaviour of U_{kk} depends on ϑ ,

$$U_{kk} \sim \begin{cases} 2D_\infty + C_{k1}^\infty(\vartheta) \omega_k^\vartheta + \dots + C_{k3}^\infty \omega_k^3, & 0 < \vartheta < 3 \\ 2D_\infty - C_{k2}^\infty \omega_k^3 \ln \omega_k\tau + C_{k4}^\infty \omega_k^3, & \vartheta = 3 \\ 2D_\infty + C_{k3}^\infty \omega_k^3 + \dots + C_{k1}^\infty(\vartheta) \omega_k^\vartheta, & 3 < \vartheta \end{cases} \quad (\text{S.58})$$

where

$$\begin{aligned} C_{k1}^\infty(\vartheta) &= (4\varpi_k^{2-\vartheta} M[h_{kk}; \vartheta + 1]/\pi) c_\infty & C_{k3}^\infty &= 8\tau^3 D_0 M[f; -3]/\pi\varpi_k \\ C_{k2}^\infty &= (4/\pi\varpi_k) c_\infty & C_{k4}^\infty &= C_{k2}^\infty [\ln \varpi_k + 2D_0 K_{k10}^1 \tau^3/c_\infty]. \end{aligned}$$

Similarly, the expansion of U_{k0} in the high-frequency limit is

$$U_{k0} \sim 2D_0 - C_{01}^0 \omega_k^{-1/2} + \dots + C_{02}^0 \omega_k^{-1}, \quad \omega_k\tau \rightarrow \infty \quad (\text{S.59})$$

with

$$C_{01}^0/c_0 = 8k^{1/2}/3 + a_{sk}/\varpi_k = A_{01}^0 \quad C_{02}^0 = 2\varpi_k D_0 M[f; 1]/\pi\tau.$$

When $\omega_k\tau \rightarrow 0$,

$$U_{k0} \sim \begin{cases} 2D_\infty + C_{01}^\infty(\vartheta) \omega_k^\vartheta + \dots + C_{03}^\infty \omega_k^3, & 0 < \vartheta < 3 \\ 2D_\infty - C_{02}^\infty \omega_k^3 \ln \omega_k\tau + C_{04}^\infty \omega_k^3, & \vartheta = 3 \\ 2D_\infty + C_{03}^\infty \omega_k^3 + \dots + C_{01}^\infty(\vartheta) \omega_k^\vartheta, & 3 < \vartheta \end{cases} \quad (\text{S.60})$$

where

$$\begin{aligned} C_{01}^\infty(\vartheta) &= -(2\varpi_k^{2-\vartheta} M[h_{k0}; \vartheta + 1]/\pi) c_\infty & C_{03}^\infty &= -4\tau^3 D_0 M[f; -3]/\pi\varpi_k \\ C_{02}^\infty &= -(2/\pi\varpi_k) c_\infty & C_{04}^\infty &= C_{02}^\infty [\ln \varpi_k + 2D_0 K_{010}^1 \tau^3/c_\infty]. \end{aligned}$$

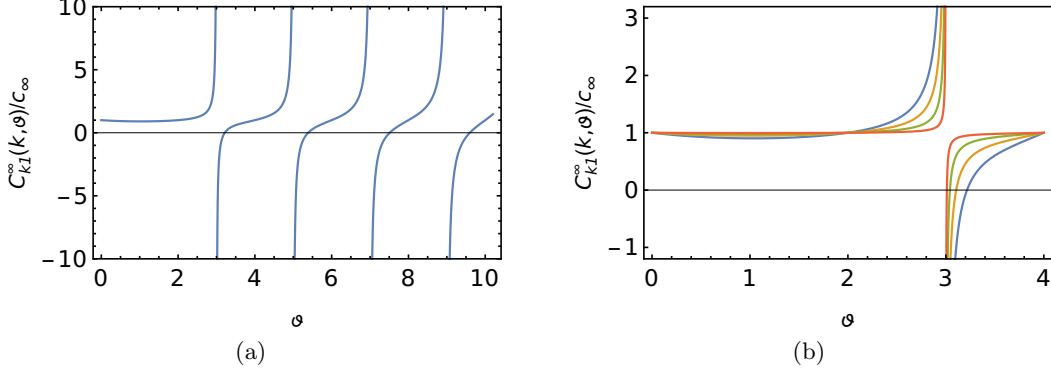


Figure S.7: Plots illustrating the characteristics of $C_{k1}^\infty(k, \vartheta)/c_\infty$ as a function of ϑ and k . (a) Plot of $C_{k1}^\infty(k, \vartheta)/c_\infty$ for $k = 1$. The singularities at $\vartheta = 3, 5, 7 \dots$ correspond to the poles of $M[h_{kk}; \vartheta + 1]$, while the region $0 < \vartheta < 3$ lies within the analytic strip of the same function. $C_{k1}^\infty(k, \vartheta)/c_\infty$ resembles $1 + \tan(\pi\vartheta/2)$ for $\vartheta > 2$. (b) Magnification of the region $0 < \vartheta < 4$ to demonstrate how $C_{k1}^\infty(k, \vartheta)/c_\infty$ behaves as a function of k . There are curves for $k = 1$ (blue), 2 (orange), 5 (green) and 20 (dark orange). Apart from the singularities, $C_{k1}^\infty(k, \vartheta)/c_\infty$ always goes to 1. There are some special cases at $\vartheta = 0, 2, 4 \dots$ where $C_{k1}^\infty(k, \vartheta)/c_\infty = 1$ independent of k , but otherwise $C_{k1}^\infty(k, \vartheta)/c_\infty$ approaches the limit as k^{-1} for increasing k .

S-7. Behaviour of $C_{k1}^\infty(k, \vartheta)$ & $C_{01}^\infty(k, \vartheta)$

It is of interest to consider how the coefficients $C_{k1}^\infty(k, \vartheta)$ & $C_{01}^\infty(k, \vartheta)$ behave with respect to ϑ and k . The coefficients may be evaluated exactly using Eqs. (S.33) & (S.34) together with some of the results for $H(s; t, c)$ and $I(s; t, c)$ in Sec. S-10.

Figure S.7 showcases the dependence of $C_{k1}^\infty(k, \vartheta)/c_\infty$ on ϑ and k . The singularities at $\vartheta = 3, 5, 7 \dots$ correspond to the poles of $M[h_{kk}; \vartheta + 1]$, while the the region $0 < \vartheta < 3$ falls within the analytic strip of the same function. Many of the characteristics of the figure can be understood by considering the large k behaviour of the coefficient. After setting $s = \vartheta + 1$ and multiplying Eq. (S.36) by $B_{kk}\varpi_k^{-\vartheta}$,

$$\frac{C_{k1}^\infty(k, \vartheta)}{c_\infty} \sim 1 + \frac{(\vartheta - 1) \tan(\pi\vartheta/2)}{\varpi_k} - \frac{2 \sec(\pi\vartheta/2)}{\Gamma(-\vartheta)} \varpi_k^{-\vartheta-2} \{1 + O(\varpi_k^{-2})\}. \quad (\text{S.61})$$

For $\vartheta > 0$, the $O(\varpi_k^{-1})$ term always dominates the $O(\varpi_k^{-\vartheta-2})$ term. $C_{k1}^\infty(k, \vartheta)$ is always exactly 1 for $\vartheta = 0, 2, 4 \dots$, which is evidenced by the plots at different k converging to the same point in Fig. S.7b, but otherwise the coefficient approaches 1 as $1/k$ for increasing k . There is also a special case where Eq. (S.61) must be evaluated in the limit $\vartheta \rightarrow 1$ so that

$$\frac{C_{k1}^\infty(k, 1)}{c_\infty} \sim 1 - \frac{2}{\pi\varpi_k} + \frac{4}{\pi\varpi_k^3} + O(\varpi_k^{-5}). \quad (\text{S.62})$$

The dominance of the $O(\varpi_k^{-1})$ term is why $C_{k1}^\infty(k, \vartheta)$ resembles plots of $1 + \tan(\pi\vartheta/2)$ for $\vartheta > 2$ (Fig. S.7a).

Figure S.8 presents $C_{01}^\infty(k, \vartheta)/c_\infty$ as a function of ϑ and k . The singularities at $\vartheta = 3, 5, 7 \dots$ correspond to the poles of $M[h_{k0}; \vartheta + 1]$, while the region $0 < \vartheta < 3$ lies within the analytic strip of the same function. Setting $s = \vartheta + 1$ and multiplying Eq. (S.35) by $B_{k0}\varpi_k^{-\vartheta}$, the following large k expansion can be derived

$$\frac{C_{01}^\infty(k, \vartheta)}{c_\infty} \sim -\frac{\tan(\pi\vartheta/2)}{\varpi_k} + \frac{\sec(\pi\vartheta/2)}{\Gamma(2 - \vartheta)} \varpi_k^{-\vartheta} \{1 + O(\varpi_k^{-2})\}. \quad (\text{S.63})$$

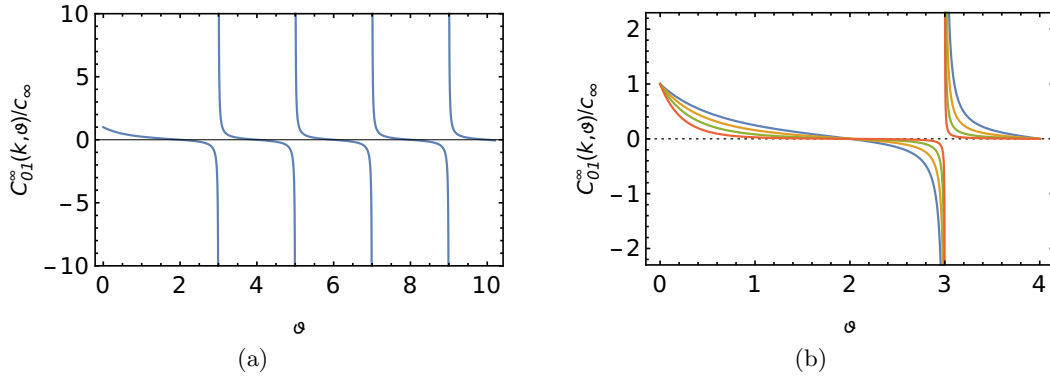


Figure S.8: Plots showcasing the features of $C_{01}^{\infty}(k, \vartheta)/c_{\infty}$ as a function of ϑ and k . (a) Plot of $C_{01}^{\infty}(k, \vartheta)/c_{\infty}$ for $k = 1$. The singularities at $\vartheta = 3, 5, 7 \dots$ correspond to the poles of $M[h_{k0}; \vartheta + 1]$, while the region $0 < \vartheta < 3$ falls within the analytic strip of the same function. $C_{01}^{\infty}(k, \vartheta)/c_{\infty}$ looks like $-\tan(\pi\vartheta/2)$ for $\vartheta > 2$. (b) Replot of the region $0 < \vartheta < 4$ to demonstrate how $C_{01}^{\infty}(k, \vartheta)/c_{\infty}$ behaves as a function of k . Curves for $k = 1$ (blue), 2 (orange), 5 (green) and 20 (dark orange) are shown. There are some special cases that are independent of k ; that is, $C_{01}^{\infty}(k, \vartheta)/c_{\infty}$ is equal to 1 for $\vartheta = 0$, and equal to 0 for $\vartheta = 2, 4, 6 \dots$. Otherwise, apart from the singularities, $C_{01}^{\infty}(k, \vartheta)/c_{\infty}$ always goes to 0 for increasing k but the way it does so depends on the value of ϑ . The limit is approached as $k^{-\vartheta}$ for $0 < \vartheta < 1$, as $k^{-1} \ln k$ for $\vartheta = 1$, and as k^{-1} for $\vartheta > 1$.

This expression resembles Eq. (S.61) in several ways, but on this occasion the large k behaviour depends on the value of ϑ :

- $\vartheta = 0$. Although this case is not relevant to the asymptotic behaviour of U_{k0} , for completeness it is mentioned that $C_{01}^{\infty}(k, 0) = 1$ independent of k .
- $0 < \vartheta < 1$. The $O(\varpi_k^{-\vartheta})$ term is dominant here so $C_{01}^{\infty}(k, \vartheta)$ goes to zero as $k^{-\vartheta}$.
- $\vartheta = 1$. Taking the limit of Eq. (S.63) as $\vartheta \rightarrow 1$ produces the finite result

$$\frac{C_{01}^{\infty}(k, 1)}{c_{\infty}} \sim \frac{2 \ln \varpi_k}{\pi \varpi_k} + \frac{2\gamma_e}{\pi \varpi_k} + O(\varpi_k^{-3}), \quad (\text{S.64})$$

which aligns with the fact that $M[h_{k0}; \vartheta + 1]$ has no pole at $\vartheta = 1$. The coefficient approaches zero as $\ln k/k$ for large k .

- $\vartheta > 1$. The $O(\varpi_k^{-1})$ term dominates for this range of ϑ , and that is why the plot in Fig. S.8a closely reflects the characteristics of $-\tan(\pi\vartheta/2)$. $C_{01}^{\infty}(k, \vartheta)$ always approaches 0 as $1/k$ except when $\vartheta = 2, 4, 6 \dots$, in which case the coefficient equals 0 independent of k .

S-8. Some comments on two previous derivations of the ADC in the high-frequency limit

I. Reference [10].

The derivation in [10] is based on equating the ADC signal model with the second order term of the cumulant expansion framework for describing DWI. After some manipulation the relationship was written in terms of the cumulative diffusion coefficient, $D(t)$, like so

$$b\tilde{D}_G(t) = \frac{\gamma^2}{2} \int_0^t d\tau_1 \int_0^{\tau_1} d\tau_2 g(\tau_1)g(\tau_2)(\tau_1 - \tau_2)D(\tau_1 - \tau_2).$$

Table S.3: Translating between the notations and conditions used in References [10] & [11] and the present manuscript.

| Quantity | Ref. [10] | Ref. [11] | Present work |
|----------------------------------|------------------------|----------------------------------|--------------------------------|
| number of oscillations | N | N | k |
| MPG duration | t | T | T |
| MPG frequency | ω | ω_0 | ω_k |
| generic time variables | τ, τ_1, τ_2 | t | t, t_1, t_2 |
| MPG amplitude | g_0 | g_0/γ | G |
| MPG phase | φ | φ | ϕ |
| cumulative diffusion coefficient | $D(t)$ | $D(T)$ | $D(T)$ |
| characteristic diffusion-time | t_D | | τ |
| finite- N correction factor | $c'(\varphi, N)$ | $\tilde{c}(\varphi, N)/\sqrt{2}$ | $\sqrt{2} C_0(k, \phi)/c_0$ |
| apparent diffusion coefficient | $\tilde{D}_G(t)$ | $-\frac{\ln s}{b}$ | $\text{ADC}_k(\phi)$ |
| strict condition | $t \ll t_D$ | $(S/V)\sqrt{D_0 T} \ll 1$ | $\beta = T/\tau \rightarrow 0$ |
| weak condition | $t/N \ll t_D$ | $(S/V)\sqrt{D_0/\omega_0} \ll 1$ | $k \rightarrow \infty$ |

The well-known expression for $D(t)$ in the short-time limit

$$D(t) = D_0 \left[1 - \frac{4}{3\sqrt{\pi}} \left(\frac{t}{t_D} \right)^{1/2} \right], \quad (\text{S.65})$$

which is said to be valid under the condition that the time t is much smaller than the characteristic time $t_D = d^2/(S/V)^2 D_0$, was then directly inserted under the integral. With $g(\tau) = g_0 \cos(\omega\tau - \varphi)$, the integrals were evaluated to finally obtain

$$\tilde{D}_G(t = 2\pi N/\omega) = D_0 \left[1 - \frac{c'(\varphi, N)}{(\omega t_D)^{1/2}} \right] \quad (\text{S.66})$$

where

$$c'(\varphi, N) = \frac{32\pi N^{3/2} \sin^2 \varphi + 12\pi N C(2N^{1/2}) + 3(3 + 4 \sin^2 \varphi) S(2N^{1/2})}{6\sqrt{2}\pi N(1 + 2 \sin^2 \varphi)},$$

and $C(x)$ and $S(x)$ are the Fresnel integrals.

The approach taken in the present manuscript starts with the same assumed equivalence between the ADC and cumulant expansion signal models. However, rather than working with a time-dependent diffusion metric, the cumulant expansion term is transformed so that the ADC is written as an integral involving the frequency-dependent metric $u_2(\omega)$ (i.e. Eq. (27) in [7] with U_{kk} & U_{k0} replaced by their integral definitions). The high-frequency asymptotic behaviour of $u_2(\omega)$ was previously known from its derivation in [6], and with that information the MTM was applied under the condition $\beta = T/\tau \rightarrow 0$ to derive asymptotic expansions for U_{kk} & U_{k0} and eventually Eq. (31) in Sec. 5.1.

To compare the two derivations it is helpful to first translate the separate notations. Table S.3 provides a map between the notations and conditions used in each study. Also, although τ has

been used in this work as a nonspecific time-scale characterising the response of a system, it could be taken as equivalent to the quantity t_D in the short-time expansion of $D(t)$. All other quantities, such as D_0 , S/V and d , have the same meaning in both studies. After applying the translation it is found that the expression for $\tilde{D}_G(t = 2\pi N/\omega)$ in Eq. (S.66) is equivalent to the result derived for $\text{ADC}_k(\phi)$ in Eq. (31). In particular, the quantity $c'(\varphi, N)$ is equivalent to $\sqrt{2}C_0(k, \phi)/c_0$.

Even though the results of the two studies are equivalent, several additional comments on differences between the works and other issues are included below:

1. The author of [10] did not anticipate any practical restrictions on the parameters of an oscillating MPG. It also seems that oscillating-gradient DWI was thought of as an experiment where N is set first, and then the duration of the MPG is varied to increase or decrease the frequency ω . Within that conceptual set-up the observer would be able to arbitrarily set the observation frequency without limitation to observe the high-frequency regime for any system.

In contrast, the present study began with the realisation that the number of oscillations and duration of an MPG are limited in practice, which means that the resolution and range of the frequency ω_k is restricted. To maximise the spectral range and resolution it was suggested in [7] that experiments are conducted by setting the duration to be as long as possible, and then the frequency is altered by varying the number of oscillations. It is possible to set the number of oscillations and then alter the MPG duration to change the frequency as conceived in [10], but the window of accessible frequencies will be unaltered. Overall, the practical restrictions on ω_k mean that the system response can only be observed within a limited immovable window of frequencies, and whether the observed response is in the high-frequency regime or otherwise depends on the nature of the system.

2. It was stated after Eq. (17) in [10] that the condition $c'(\varphi, N)(\omega t_D)^{-1/2} \ll 1$ must be satisfied for Eq. (S.66) to be a valid asymptotic expansion. This condition and the large N behaviour of $c'(\varphi, N)$ led the author of [10] to conclude that the critical time-scale depends on the waveform selected for the applied MPG. More explicitly, after substituting $\omega = 2\pi N/t$ the condition becomes $[c'(\varphi, N)/(2\pi N)^{1/2}](t/t_D)^{1/2} \ll 1$. Since $c'(\varphi, N)$ is $O(N^{1/2})$ for large N and $\varphi \neq 0$, the condition therefore implies that the high-frequency expansion of the ADC is valid if $t \ll t_D$. On the other hand, $c'(\varphi, N)$ is $O(1)$ for the special case $\varphi = 0$, which means that the expansion is valid for the weaker condition $t/N \ll t_D$. That is, non-cos-type MPGs require the duration of the whole MPG to be dominated by the characteristic diffusion-time, whereas for cos-type MPGs only the period of the oscillations needs to be much smaller than the characteristic diffusion-time.

In comparison, the derivations in this work assume from the beginning that $T/\tau \rightarrow 0$, which is equivalent to the stricter condition of [10]. Nevertheless, given the equivalence between $c'(\varphi, N)$ and $\sqrt{2}C_0(k, \phi)/c_0$, if ϕ is set to zero in Eq. (31) then the same reasoning as used in [10] can be applied to obtain the weak condition $T/k \ll \tau$ for cos-type MPGs.

3. There is a small error in Eq. (17) of [10]. It was stated that $c'(0, N) = (1/\sqrt{2})(1 - 1/\pi^2 N^{3/2})$ for $N \gg 1$, whereas the expression should actually be $c'(0, N) = (1/\sqrt{2})(1 + 3/4\sqrt{2}\pi N)$. The factor of $-1/\pi^2 N^{3/2}$ actually appears in the third term of the large N expansion of $c'(0, N)$.
4. The quantity k in Eqs. (19), (21) & (22) of [10] was never defined.

II. Reference [11].

Even though the ADC is not explicitly mentioned in [11], the high-frequency behaviour of the signal observed using an MPG with a finite number of oscillations is discussed in Appendix C. The discussion is based on a signal equation derived in the preceding appendix, Appendix B. That equation, Eq. (B5), was written in terms of the time-dependent diffusion metrics $\mathcal{D}(t)$, the retarded velocity autocorrelation function, and $D(T)$, the cumulative diffusion coefficient.³ Expressions for $\mathcal{D}(t)$ and $D(T)$ in the short-time limit were inserted into Eq. (B5) and the integrals were evaluated. The final result, Eq. (C6), is equivalent to the result obtained in Ref. [10] (i.e. Eq. (S.66) above), and hence it is also equivalent to the result presented in this work.

Some additional remarks on [11] are listed below:

1. In the paragraph after Eq. (C6) it is mentioned that the finite- N correction factor, $\tilde{c}(\varphi, N)$ (see Table S.3 for the translation between studies), diverges as $N^{1/2}$ for large N . This is the same issue that was highlighted by the author of [10]. The authors of [11] point out that the problem of divergence only arises when the strict condition, $(S/V)\sqrt{D_0T} \ll 1$, is violated. It is also noted that the $N^{1/2}$ dependence is due to the factor of $T^{1/2}$ in the short-time expansion of $D(T)$ and subsequently “forcing Eq. (C6) to mimic the form of Eq. (32).”⁴ A similar situation occurs in the current manuscript. The $O(k^{1/2})$ term in A_{01}^0 originates from writing the high-frequency asymptotic behaviour of U_{k0} (re Eq. (27)) in terms of $\omega_k\tau$ instead of the true asymptotic variable β . The present authors agree that the problem of divergence is spurious and will not occur as long as the strict condition, $\beta \rightarrow 0$, holds.
2. A physical interpretation for the log signal as the sum of a pure oscillating gradient (OG) component and a pulsed gradient (PG) component is discussed in [11]. The OG component corresponds to the signal when $\varphi = 0$, while the PG component is the additional signal that appears when φ is nonzero. The authors of [11] propose that the decomposition into components allows Eq. (C4) to be used to probe the S/V limit for any value of φ as long as the weak condition, $(S/V)\sqrt{D_0/\omega_0} \ll 1$, is met. This is in contrast to the conclusion in [10] where the weak condition only applies when $\varphi = 0$.

In the notation of the present manuscript the OG & PG components correspond to U_{kk} & U_{k0} , respectively. Recalling that $A_{k1}^0 \sim O(1)$, the same reasoning as used in [11] with respect to Eq. (C4) could be applied here to argue that under suitable conditions the U_{kk} contribution to Eq. (2) may probe the high-frequency limit regardless of the behaviour of the U_{k0} contribution. This is an interesting idea, but its application is hindered by the practical limitations on MPG duration and frequency. It is also unclear how the OG contribution to the signal could be reliably isolated when $\phi \neq 0$.

3. There is some potential for confusion in [11] with regards to how the asymptotic results derived from Eq. (B5) in Appendix B and Appendix C are obtained.

The derivation in Appendix C proceeds by directly inserting Eq. (C1) into Eq. (B5) without indicating what the asymptotic variable is. However, as the result is equivalent to that obtained here using the MTM, it can be concluded that the asymptotic variable in the derivation of Appendix C must be T (with N kept constant).⁵ That is, similar to what has been done in

³The equivalence of Eq. (B5) and Eq. (2) was previously addressed in the Supporting Material (Sec. S-9) of [7].

⁴Eq. (32) of [11] is the short-time expansion of $D(t)$. The authors probably meant Eq. (33), which is the high-frequency expansion of $\text{Re } \mathcal{D}(\omega)$.

⁵Even though $\beta = T/\tau$ was the asymptotic variable used in this work, the effective asymptotic quantity is T because τ , which is a property of the sample, is constant.

this manuscript, Eq. (C6) is an asymptotic expansion of the signal as $T \rightarrow 0$ that is written in terms of the frequency ω_0 (using the fact $T = 2\pi N/\omega_0$).

On the other hand, it was previously noted in [7] (Supplementary Material, Sec. S-9) that Eq. (B6) was derived from Eq. (B5) under the assumption that ω_0 remains constant. Since $\omega_0 = 2\pi N/T$, the assumption means that N and T are a coupled set of asymptotic variables. That is, the asymptotic behaviour is obtained by replacing every occurrence of N with $\omega_0 T/2\pi$ (or T with $2\pi N/\omega_0$) and expanding as T goes to 0 (or N goes to ∞). Deriving the expansion in this way produces a different result to when T and N are uncoupled. For example, using the exact U_{k0} & U_{kk} calculated for Model 2 in [7], the asymptotic behaviour with T and k coupled is:

$$\begin{aligned}\frac{U_{k0}}{2D_0} &\sim 1 - \zeta + \frac{2\zeta(\omega_k\tau)^{1/2}}{\pi^{1/2}} \varpi_k^{-1/2} - \frac{\zeta(\omega_k\tau)^{1/2}}{\sqrt{2}} \left[\frac{1 + \omega_k\tau + \sqrt{2}(\omega_k\tau)^{5/2}}{1 + (\omega_k\tau)^2} \right] \varpi_k^{-1} + O(\varpi_k)^{-3/2} \\ \frac{U_{kk}}{2D_0} &\sim u_2(\omega_k) - \frac{\zeta(\omega_k\tau)^{1/2}}{\sqrt{2}} \left[\frac{1 - \omega_k\tau + 5(\omega_k\tau)^2 - 8(\omega_k\tau)^{5/2} + 3(\omega_k\tau)^3}{2[1 + 2(\omega_k\tau)^2]^2} \right] \varpi_k^{-1} + O(\varpi_k)^{-5/2}.\end{aligned}$$

Comparison of these expressions with the $\omega_k\tau \rightarrow \infty$ parts of Eqs. (22) & (23), which were derived with β as the sole asymptotic variable, finds that the results are quite different. In particular, notice that the lowest order term in U_{kk} is $u_2(\omega_k)$, which is not the case in Eq. (23).

4. The present authors are also aware that the asymptotic behaviour of the signal might be investigated in a third way. In Sec. 2.1 it was noted that ω_k may be manipulated by independently varying either k or T , but practical limitations restrict the range of both quantities. It was therefore argued that it is the ratio of T and the characteristic time-scale τ that determines the regime for OGSE-DWI observations. Varying k provides only a small perturbation to the observed response because the range of k is limited. However, if the practical limitation on k could be ignored, increasing k (with constant T) would concurrently decrease the period of the oscillation so that the condition for the high-frequency limit, $\omega_k\tau = 2\pi k\tau/T \rightarrow \infty$, is eventually satisfied. That is, the high-frequency limit of the sample is probed under the condition $k \rightarrow \infty$, which is a form of the weak condition because it implies that the period of the oscillation, T/k , is the critical time-scale. In general, the asymptotic expansions of U_{k0} , U_{kk} and the ADC obtained in this way differ from the results obtained under the strict condition. The exact U_{k0} & U_{kk} for Model 2 of [7] are used to demonstrate this:

$$\begin{aligned}\frac{U_{k0}}{2D_0} &\sim 1 - \zeta - \zeta \frac{1 - 2\sqrt{\beta/\pi} - e^\beta \operatorname{erfc}(\sqrt{\beta})}{\beta} - \frac{\zeta}{\sqrt{2}\beta} (\omega_k\tau)^{-3/2} + O(\omega_k\tau)^{-2} \\ \frac{U_{kk}}{2D_0} &\sim 1 - \frac{\zeta}{\sqrt{2}} (\omega_k\tau)^{-1/2} - \frac{\zeta(3 - 2\beta)}{2\sqrt{2}\beta} (\omega_k\tau)^{-3/2} + O(\omega_k\tau)^{-2}.\end{aligned}$$

These expansions have been written in terms of powers of $\omega_k\tau$ to aid comparison with the high-frequency results of Eqs. (22)–(23) in Sec. 3. One obvious difference is that the coefficients to the powers of $\omega_k\tau$ here are functions of β , whereas the coefficients in Eqs. (19), (20), (22) & (23) feature k (or ϖ_k) but not β . This is consistent with the fact that the asymptotic variable here is k , while the actual asymptotic variable used for the results in Sec. 3 is β . With future improvements in gradient hardware it might become possible to implement MPGs with very high values of k . Even so, there are other issues (e.g. high SAR, insufficient diffusion-weighting

or signal attenuation) that might prevent the use of large k . So, although it might be possible in principle, probing the high-frequency/short-time limit in this way does not seem to be practical.

5. There is a typographical error in the upper part of Eq. (C2) in [11]. Rather than $\sqrt{2}/\omega_0[\dots]$, the right-hand side should be $\sqrt{2/\omega_0}[\dots]$. The subsequent results have not been affected by this error.

S-9. Low-frequency asymptotic behaviour of the ADC for a single-harmonic MPG

For a single-harmonic MPG the ADC can be written in terms of U_{kk} & U_{k0} as [7]

$$\text{ADC}_k(\phi) = \frac{U_{kk} + 2U_{k0} \sin^2 \phi}{2 + 4 \sin^2 \phi}. \quad (\text{S.67})$$

One way to determine the low-frequency behaviour of the ADC is to insert the appropriate asymptotic expressions for U_{k0} & U_{kk} from Sec. 4.2. However, that approach is problematic due to the dependence of the results on ϑ . For example, as ϑ approaches 3 from below $C_{k1}^\infty(k, \vartheta) \rightarrow +\infty$ while $C_{01}^\infty(k, \vartheta) \rightarrow -\infty$, so it is not immediately clear which behaviour will dominate in the asymptotic behaviour of the ADC. This problem could be solved with some careful analysis, but a more straightforward method is to rewrite Eq. (S.67) as an integral and then apply the MTM.

An integral expression for the ADC is constructed by introducing the integral definitions of U_{k0} & U_{kk} into Eq. (S.67) so that

$$\text{ADC}_k(\phi) = \frac{1}{2} \int_0^\infty d\omega u_2(\omega) H_k(\omega; T, \phi) \quad (\text{S.68})$$

with

$$H_k(\omega; T, \phi) = \frac{H_{kk}(\omega; T) + 2H_{k0}(\omega; T) \sin^2 \phi}{1 + 2 \sin^2 \phi}.$$

Using the properties of the $H_{kl}(\omega; T)$ it can be shown that $\int_0^\infty d\omega H_k(\omega; T, \phi) = 1$ and $H_k(\omega; T, \phi) = B_k(\phi) T h_k(\omega T; \phi)$, where

$$h_k(v; \phi) = \frac{(1 - \cos v)[v^2 \cos^2 \phi + \varpi_k^2 \sin^2 \phi]}{v^2[v^2 - \varpi_k^2]^2}$$

and $B_k(\phi) = 4\varpi_k^2/(1 + 2 \sin^2 \phi)\pi$. It is therefore possible to rewrite Eq. (S.68) in the dimensionless form

$$I_k(\beta; \phi) = \frac{\text{ADC}_k(\phi)}{D_0 \beta B_k(\phi)} = \int_0^\infty dv f(v) h_k(\beta v; \phi) \quad (\text{S.69})$$

with $f(v) = u_2(v/\tau)/2D_0$ as in Sec. 2.2.

From here the procedure is very similar to that used in Sec. S-6 but with some of the details removed. The first step is to record the asymptotic behaviour of $h_k(v; \phi)$:

$$h_k(v; \phi) \sim \begin{cases} \sum_{n=0}^{\infty} h_n^0(\phi) v^{2n}, & v \rightarrow 0 \\ (1 - \cos v) \sum_{n=0}^{\infty} h_n^\infty(\phi) v^{-2n-4}, & v \rightarrow \infty. \end{cases}$$

Since $h_k(v; \phi) = h_{kk}(v) - h_{k0}(v) \sin^2 \phi$ it is possible to write the coefficients in these expansions as (re Secs. 2.3 & S-3)

$$h_n^0(\phi) = \begin{cases} -h_{00}^0 \sin^2 \phi, & n = 0 \\ h_{kn-1}^0 - h_{0n}^0 \sin^2 \phi, & n \geq 1 \end{cases}$$

$$h_n^\infty(\phi) = \begin{cases} \cos^2 \phi, & n = 0 \\ h_{kn}^\infty - h_{0n}^\infty \sin^2 \phi, & n \geq 1. \end{cases}$$

Notice that $h_0^0(0) = 0$ and $h_0^\infty(\pi/2) = 0$, which means that the analytic strip and poles of $M[h_k; s]$ depend on the value of ϕ . In fact, the analytic strip may be summarised as $-2\delta_{0,\phi} < \text{Re } s < 4 + 2\delta_{\pi/2,\phi}$ and the behaviour of $M[h_k; s]$ at its poles is

$$M[h_k; s] \sim \begin{cases} \frac{h_{n+\delta_{0,\phi}}^0(\phi)}{s + 2n + 2\delta_{0,\phi}}, & s \rightarrow -2n - 2\delta_{0,\phi} \\ -\frac{h_{n+\delta_{\pi/2,\phi}}^\infty(\phi)}{s - 2n - 4 - 2\delta_{\pi/2,\phi}}, & s \rightarrow 2n + 4 + 2\delta_{\pi/2,\phi} \end{cases}$$

for $n = 0, 1, 2, \dots$.

Assuming the same behaviour for $f(v)$ and its Mellin transform as in Sec. 2.3, the convergence of $I_k(\beta; \phi)$ requires that $\vartheta > -1 - 2\delta_{0,\phi}$. The expansion of $I_k(\beta; \phi)$ as $\beta \rightarrow \infty$ can therefore be broken down into the following cases:

- (a) $0 < \vartheta < 3 + 2\delta_{\pi/2,\phi}$. The analytic strips of $M[f_1; 1-s]$ and $M[f_2; 1-s]$ intersect with that of $M[h_k; s]$ for $-1 - 2\delta_{0,\phi} < \text{Re } s < 1$ and $1 < \text{Re } s < 4 + 2\delta_{\pi/2,\phi}$, respectively, so the corresponding known poles in the right-hand plane are

$$\{s_n \geq 1\} = \{2n + 4 + 2\delta_{\pi/2,\phi}\} \cup \{1, \vartheta + 1\} = \{1, \vartheta + 1, \dots, 4 + 2\delta_{\pi/2,\phi}, \dots\}$$

$$\{s_n \geq 4 + 2\delta_{\pi/2,\phi}\} = \{2n + 4 + 2\delta_{\pi/2,\phi}\} = \{4 + 2\delta_{\pi/2,\phi}, \dots\}.$$

There are no second order poles so the residues are easily calculated and

$$I_k(\beta; \phi) \sim \frac{D_\infty}{D_0} M[h_k; 1] \beta^{-1} + \frac{c_\infty}{2D_0 \tau^\vartheta} M[h_k; \vartheta + 1] \beta^{-\vartheta-1}.$$

- (b) $\vartheta = 3 + 2\delta_{\pi/2,\phi}$. In this case the pole at $\vartheta + 1 = 4 + 2\delta_{\pi/2,\phi}$ of $M[f_1; 1-s]$ coincides with the first pole of $M[h_{kl}; s]$. As such,

$$\{s_n \geq 1\} = \{2n + 4 + 2\delta_{\pi/2,\phi}\} \cup \{1, \vartheta + 1\} = \{1, (4 + 2\delta_{\pi/2,\phi}, 4 + 2\delta_{\pi/2,\phi}), \dots\}$$

and the expansion is

$$I_k(\beta; \phi) \sim \frac{D_\infty}{D_0} M[h_k; 1] \beta^{-1} + \frac{c_\infty h_{\delta_{\pi/2,\phi}}^\infty(\phi)}{2D_0 \tau^{3+2\delta_{\pi/2,\phi}}} \beta^{-4-2\delta_{\pi/2,\phi}} \ln \beta.$$

- (c) $\vartheta > 3 + 2\delta_{\pi/2,\phi}$. The order of the poles switches from that in case (a):

$$\{s_n \geq 1\} = \{2n + 4 + 2\delta_{\pi/2,\phi}\} \cup \{1, \vartheta + 1\} = \{1, 4 + 2\delta_{\pi/2,\phi}, \vartheta + 1, \dots\}$$

so that now

$$I_k(\beta; \phi) \sim \frac{D_\infty}{D_0} M[h_k; 1] \beta^{-1} + h_{\delta_{\pi/2,\phi}}^\infty(\phi) M[f; -3 - 2\delta_{\pi/2,\phi}] \beta^{-4-2\delta_{\pi/2,\phi}}.$$

Now recalling Eq. (S.69) and using the facts that $\beta = \varpi_k/\omega_k\tau$ and $M[h_k; s] = M[h_{kk}; s] - M[h_{k0}; s] \sin^2 \phi$, the expansion of the ADC in the low-frequency limit can be summarised as

$$\text{ADC}_k(\phi) \sim \begin{cases} D_\infty + C_1^\infty(k, \phi, \vartheta) \omega_k^\vartheta, & 0 < \vartheta < 3 + 2\delta_{\pi/2, \phi} \\ D_\infty - C_2^\infty(k, \phi) \omega_k^{3+2\delta_{\pi/2, \phi}} \ln \omega_k \tau, & \vartheta = 3 + 2\delta_{\pi/2, \phi} \\ D_\infty + C_3^\infty(k, \phi) \omega_k^{3+2\delta_{\pi/2, \phi}}, & \vartheta > 3 + 2\delta_{\pi/2, \phi} \end{cases}$$

where

$$\begin{aligned} \frac{C_1^\infty(k, \phi, \vartheta)}{c_\infty} &= \frac{2\varpi_k^{2-\vartheta}}{(1 + 2\sin^2 \phi)\pi} M[h_k; \vartheta + 1] \\ \frac{C_2^\infty(k, \phi)}{c_\infty} &= \frac{2\varpi_k^{-1-2\delta_{\pi/2, \phi}}}{(1 + 2\sin^2 \phi)\pi} h_{\delta_{\pi/2, \phi}}^\infty(\phi) \\ \frac{C_3^\infty(k, \phi)}{D_0} &= \frac{2\varpi_k^{-1-2\delta_{\pi/2, \phi}}}{(1 + 2\sin^2 \phi)\pi} h_{\delta_{\pi/2, \phi}}^\infty(\phi) M[f; -3 - 2\delta_{\pi/2, \phi}] \tau^{3+2\delta_{\pi/2, \phi}}. \end{aligned}$$

For $\phi = 0$, the result is equivalent to the expansion of $U_{kk}/2$ as expected. In particular, $C_1^\infty(k, 0, \vartheta) = C_{k1}^\infty(k, \vartheta)/2$, $C_2^\infty(k, 0) = C_{k2}^\infty(k)/2$ and $C_3^\infty(k, 0) = C_{k3}^\infty(k)/2$.

For $0 < \phi < \pi/2$, the analytic strip of $M[h_k; \vartheta + 1]$ narrows to $-1 < \vartheta < 3$. That is, a pole that did not exist for $\phi = 0$ appears at $\vartheta = -1$, which corresponds to the fact that $h_0^0(\phi) \neq 0$ when $\phi \neq 0$.

For $\phi = \pi/2$, the pole of $M[h_k; \vartheta + 1]$ at $\vartheta = 3$ disappears because $h_0^\infty(\pi/2) = 0$. This broadens the analytic strip of $M[h_k; \vartheta + 1]$ to $-1 < \vartheta < 5$, and also indicates that the divergences in $C_{k1}^\infty(k, \vartheta)$ and $C_{01}^\infty(k, \vartheta)$ cancel each other when $\phi = \pi/2$. Figure S.9 illustrates the behaviour of $C_1^\infty(k, \pi/2, \vartheta)$ with respect to ϑ and k . Many features of the figure can be qualitatively understood using the large k expansion

$$\frac{6C_1^\infty(k, \pi/2, \vartheta)}{c_\infty} \sim 1 + \lim_{\vartheta' \rightarrow \vartheta} \left\{ \frac{(\vartheta' - 3) \tan(\pi\vartheta'/2)}{\varpi_k} + \frac{2 \sec(\pi\vartheta'/2)}{\Gamma(2 - \vartheta')} \varpi_k^{-\vartheta'} + O(\varpi_k^{-\vartheta'-2}) \right\}.$$

Overall, for $\vartheta > 0$ it is found that

$$C_1^\infty(k, \pi/2, \vartheta) \omega_k^\vartheta \sim O(\varpi_k^\vartheta),$$

which means that plots of the ADC against ω_k will tend towards the apparent dependence on frequency.

S-10. Various integrals

A number of integrals used in the preceding sections are evaluated here.

1. Letting s be a complex number such that $0 < \text{Re } s < 1$, and $a \neq 0$ be any complex number that does not lie on the positive real axis, consider the integral

$$J(s; a) = \oint_C dz \frac{z^{s-1}}{z+a} \quad (\text{S.70})$$

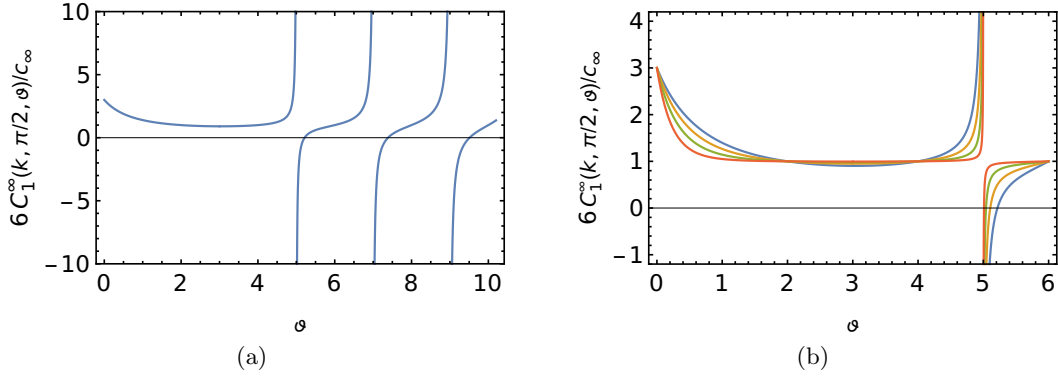


Figure S.9: Plots illustrating the characteristics of $C_1^\infty(k, \pi/2, \vartheta)/c_\infty$ as a function of ϑ and k for $\phi = \pi/2$. (a) Plot of $C_1^\infty(k, \pi/2, \vartheta)/c_\infty$ for $k = 1$. The singularities at $\vartheta = 5, 7, 9 \dots$ correspond to the poles of $M[h_k; \vartheta + 1]$, and the singularity-free region $0 < \vartheta < 5$ is within the analytic strip of the same function. $C_1^\infty(k, \pi/2, \vartheta)/c_\infty$ resembles $C_{k1}^\infty(\vartheta, \pi/2)/c_\infty$ for $\vartheta > 5$ (re Fig. S.7). (b) Magnification of the region $0 < \vartheta < 6$ with curves for $k = 1$ (blue), 2 (orange), 5 (green) and 20 (dark orange). For $\vartheta > 0$, $6C_1^\infty(k, \pi/2, \vartheta)/c_\infty$ always goes to 1 for increasing k but the way it does so depends on the value of ϑ . The limit is approached as $k^{-\vartheta}$ for $0 < \vartheta < 1$, as $k^{-1} \ln k$ for $\vartheta = 1$, and as k^{-1} for $1 < \vartheta$. There are also some special cases that are independent of k ; that is, $6C_1^\infty(k, \pi/2, \vartheta)/c_\infty$ is equal to 3 for $\vartheta = 0$, and equal to 1 for $\vartheta = 2, 4, 6 \dots$.

around the contour C shown in Fig. S.10. The condition on the real part of s ensures that the integrals around the two circular segments will both be zero in the limits $\epsilon \rightarrow 0$ and $R \rightarrow \infty$. The remaining contributions give

$$J(s; a) = \int_0^\infty dx \frac{x^{s-1}}{x+a} + \int_\infty^0 dx \frac{x^{s-1} e^{2\pi i(s-1)}}{x+a} = 2\pi i \operatorname{Res} \left\{ \frac{z^{s-1}}{z+a} \right\}_{z=-a} = 2\pi i (-a)^{s-1}.$$

After some simple algebra it is found that

$$\int_0^\infty dx \frac{x^{s-1}}{x+a} = \frac{\pi a^{s-1}}{\sin \pi s}. \quad (\text{S.71})$$

The left-hand side of this result defines the Mellin transform of $1/(x+a)$ (i.e. $M[1/(x+a); s]$), which means that even though the integral was evaluated with the restrictions on

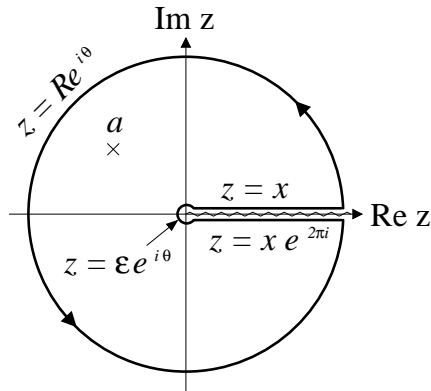


Figure S.10: Contour C used to evaluate Eq. (S.70). The contour runs either side of a branch cut drawn along the positive real axis, and a is an arbitrary complex number within the contour.

$\text{Re } s$, analytic continuation of the Mellin transform guarantees that the result holds for all $s \in \mathbb{C}$.

2. Given real constants $t \geq 0$ and $c > 0$, another integral of interest is

$$H(s; t, c) = \int_0^\infty dv \frac{v^{s-1} e^{-vt}}{v^2 + c^2} \quad (\text{S.72})$$

with $1 < \text{Re } s < 4$. Partial fraction decomposition of the denominator is first applied so that

$$H(s; t, c) = \frac{1}{2ic} \int_0^\infty dv v^{s-1} e^{-vt} \left[\frac{1}{v - ic} - \frac{1}{v + ic} \right] = \frac{\bar{J} - J}{2ic}$$

with \bar{J} representing the complex conjugate of J . For $t = 0$, Eq. (S.71) with $a = ic$ may be used to evaluate J so that the overall result simplifies to

$$H(s; 0, c) = \frac{\pi c^{s-2}}{2 \sin \pi s/2}. \quad (\text{S.73})$$

On the other hand, if $t > 0$ then

$$J = \int_0^\infty dv \frac{v^{s-1} e^{-vt}}{v + ic} = e^{ict} \int_0^\infty dv v^{s-1} \int_t^\infty db e^{-b(v+ic)} = e^{ict} \Gamma(s) \int_t^\infty db b^{-s} e^{-icb}.$$

After setting $w = cb$,

$$J = c^{s-1} e^{ict} \Gamma(s) \int_{ct}^\infty dw \frac{\cos w - i \sin w}{w^s} = c^{s-1} e^{ict} \Gamma(s) [\text{ci}(1 - s, ct) - i \text{si}(1 - s, ct)].$$

where $\text{ci}(z, t)$ and $\text{si}(z, t)$ are the upper generalised cosine and sine integrals, respectively (Sec. 8.21, Digital Library of Mathematical Functions). Some straightforward algebra subsequently finds that

$$H(s; t, c) = c^{s-2} \Gamma(s) [\text{si}(1 - s, ct) \cos ct - \text{ci}(1 - s, ct) \sin ct]. \quad (\text{S.74})$$

As $H(s; t, c)$ is the Mellin transform of $e^{-vt}/(v^2 + c^2)$, it can be analytically continued into the whole complex plane to be a meromorphic function with poles at $s = -n$, $n = 0, 1, 2, \dots$.

When s takes on positive integer values (i.e. $s = n$, $n = 1, 2, \dots$) or half-integer values (i.e. $s = n + 1/2$, $n \in \mathbb{Z}$), the generalised sine and cosine integrals may be written in terms of simpler functions. For example, for nonzero t and $s = 1$

$$\text{ci}(0, ct) = \int_{ct}^\infty dw \frac{\cos w}{w} = -\text{Ci}(ct)$$

$$\text{si}(0, ct) = \int_{ct}^\infty dw \frac{\cos w}{w} = \left\{ \int_0^\infty - \int_0^{ct} \right\} dw \frac{\sin w}{w} = \frac{\pi}{2} - \text{Si}(ct)$$

where $\text{Ci}(x)$ and $\text{Si}(x)$ are the standard cosine and sine integrals, respectively, and $\text{Si}(\infty) = \pi/2$ has been used. Subsequently,

$$H(1; t, c) = \frac{1}{c} \left\{ \left[\frac{\pi}{2} - \text{Si}(ct) \right] \cos ct + \text{Ci}(ct) \sin ct \right\}. \quad (\text{S.75})$$

Similarly, when $s = 1/2$ the variable change $w = \pi u^2/2$ can be applied to show that

$$\begin{aligned} \text{ci}(1/2, ct) &= \int_{ct}^{\infty} dw \frac{\cos w}{\sqrt{w}} = \sqrt{2\pi} \left\{ \int_0^{\infty} - \int_0^{\sqrt{2ct/\pi}} \right\} du \cos \frac{\pi u^2}{2} = \sqrt{\frac{\pi}{2}} \left[1 - 2C(\sqrt{2ct/\pi}) \right] \\ \text{si}(1/2, ct) &= \int_{ct}^{\infty} dw \frac{\sin w}{\sqrt{w}} = \sqrt{\frac{\pi}{2}} \left[1 - 2S(\sqrt{2ct/\pi}) \right] \end{aligned}$$

where $C(x)$ and $S(x)$ are the Fresnel cosine and sine integrals, respectively, and $C(\infty) = S(\infty) = 1/2$ has been used. This means that

$$H(1/2; t, c) = \frac{\pi}{\sqrt{2}c^{3/2}} \left\{ \left[1 - 2S(\sqrt{2ct/\pi}) \right] \cos ct - \left[1 - 2C(\sqrt{2ct/\pi}) \right] \sin ct \right\}. \quad (\text{S.76})$$

It is also useful to know that differentiating $H(s; t, c)$ with respect to t finds that

$$H(s+1; t, c) = -\frac{d}{dt}H(s; t, c). \quad (\text{S.77})$$

As examples of applying this relationship,

$$\begin{aligned} H(3/2; t, c) &= -\frac{d}{dt}H(1/2; t, c) = \frac{\pi}{\sqrt{2}c^{1/2}} \left\{ \left[1 - 2C(\sqrt{2ct/\pi}) \right] \cos ct \right. \\ &\quad \left. + \left[1 - 2S(\sqrt{2ct/\pi}) \right] \sin ct \right\} \end{aligned} \quad (\text{S.78})$$

$$H(2; t, c) = -\frac{d}{dt}H(1; t, c) = \left[\frac{\pi}{2} - \text{Si}(ct) \right] \sin ct - \text{Ci}(ct) \cos ct. \quad (\text{S.79})$$

On the other hand, $H(s; t, c)$ may be evaluated for noninteger values of $\text{Re } s < 0$ by integrating Eq. (S.77) so that

$$H(s-1; t, c) = H(s-1; 0, c) - \int_0^t db H(s; b, c), \quad (\text{S.80})$$

and then using Eq. (S.73) for $H(s-1; 0, c)$.

Unfortunately, repeated differentiation and integration can be arduous. To make evaluation of $H(s; t, c)$ simpler a recursion relation can be developed by noting that

$$i^{-z}\Gamma(z, it) = \text{ci}(z, t) - i \text{si}(z, t), \quad (\text{S.81})$$

and then using the well-known identity $\Gamma(z+1, t) = t^z e^{-t} + z\Gamma(z, t)$ to show that

$$\begin{aligned} \text{ci}(z+1, t) &= -t^z \sin t - z \text{si}(z, t) \\ \text{si}(z+1, t) &= t^z \cos t + z \text{ci}(z, t). \end{aligned}$$

It follows that

$$H(s+2; t, c) = t^{-s}\Gamma(s) - c^2 H(s; t, c). \quad (\text{S.82})$$

3. Consider

$$I(s; t, c) = \int_0^\infty dv \frac{v^{s-1} e^{-vt}}{(v^2 + c^2)^2} \quad (\text{S.83})$$

for real constants $t \geq 0$ and $c > 0$, and $-1 < \text{Re } s < 4$. This integral can be evaluated by noting that

$$\frac{1}{(v^2 + c^2)^2} = -\frac{1}{2c} \frac{d}{dc} \frac{1}{(v^2 + c^2)},$$

so that it is possible to write

$$I(s; t, c) = -\frac{1}{2c} \frac{d}{dc} \int_0^\infty dv \frac{v^{s-1} e^{-vt}}{v^2 + c^2} = -\frac{1}{2c} \frac{d}{dc} H(s; t, c). \quad (\text{S.84})$$

Using the fact that

$$\begin{aligned} \frac{d}{dc} \text{si}(1 - s, ct) &= -t^{1-s} c^{-s} \sin ct \\ \frac{d}{dc} \text{ci}(1 - s, ct) &= -t^{1-s} c^{-s} \cos ct, \end{aligned}$$

it follows from Eq. (S.74) that for $t > 0$

$$\begin{aligned} I(s; t, c) &= -\frac{c^{s-4} \Gamma(s)}{2} \{ \text{si}(1 - s, ct) [(s - 2) \cos ct - ct \sin ct] \\ &\quad - \text{ci}(1 - s, ct) [(s - 2) \sin ct + ct \cos ct] \}. \end{aligned} \quad (\text{S.85})$$

Since $I(s; t, c)$ is the Mellin transform of $e^{-vt}/(v^2 + c^2)^2$, analytic continuation into the whole complex plane finds that it is a meromorphic function with poles at $s = -n$, $n = 0, 1, 2, \dots$. For the special case when $t = 0$, differentiation of Eq. (S.73) gives

$$I(s; 0, c) = -\frac{\pi(s - 2)c^{s-4}}{4 \sin \pi s/2}. \quad (\text{S.86})$$

It is also worthwhile mentioning that, similar to the case for item 2 above, a recursion relation could be derived for $I(s; t, c)$. However, a separate recursion relation for this quantity is unnecessary as it is simpler to use Eq. (S.82) followed by Eq. (S.84).

4. Mellin transform of $v^\alpha (\ln v)^p$ for $\alpha \in \mathbb{C}$ and p a finite non-negative integer. If v_0 is a finite positive real number let $f_1(v)$ be equal to $v^\alpha (\ln v)^p$ for $0 < v < v_0$ and 0 otherwise. Also, let $f_2(v) = v^\alpha (\ln v)^p - f_1(v)$. Even though the final result is true for arbitrary v_0 , for demonstration purposes it is convenient to choose $v_0 = 1$. In that case repeated integration-by-parts gives

$$\begin{aligned} \int_0^\infty dv v^{s-1} f_1(v) &= \frac{(-)^p p!}{(s + \alpha)^{p+1}}, & \text{Re } s > -\text{Re } \alpha \\ \int_0^\infty dv v^{s-1} f_2(v) &= -\frac{(-)^p p!}{(s + \alpha)^{p+1}}, & \text{Re } s < -\text{Re } \alpha. \end{aligned}$$

Analytic continuation of these results into the whole complex plane defines $M[f_1; s]$ and $M[f_2; s]$. Therefore,

$$M[v^\alpha (\ln v)^p; s] = M[f_1; s] + M[f_2; s] = 0, \quad (s \neq -\alpha) \quad (\text{S.87})$$

with the point $s = -\alpha$ being a pole.

5. The following integral identity is an edited version of the contour integral evaluated in Sec. S-1 of the Supporting Material from [7]. It is assumed that $F(z)$ is a complex function obeying the conditions:

- (i) There are no poles along the positive real and imaginary axes, nor within the first quadrant of the complex plane.
- (ii) For every $R > 0$ there is a real number $c(R)$ such that $|F(Re^{i\theta})| \leq c(R)$ and $\lim_{R \rightarrow \infty} c(R)/R = 0$.

Then, if l is either 0 or k ,

$$P \int_0^\infty dx \frac{F(x)(1 - e^{ix})}{(x^2 - \varpi_k^2)(x^2 - \varpi_l^2)} = \frac{\pi F(\varpi_k \delta_{k,l})}{2(3\delta_{k,l} - 1)\varpi_k^2} + iP \int_0^\infty dy \frac{F(iy)(1 - e^{-y})}{(y^2 + \varpi_k^2)(y^2 + \varpi_l^2)}. \quad (\text{S.88})$$